

Fully distributed and resilient source seeking for robot swarms

Jesus Bautista*, *Student, IEEE*, Antonio Acuaviva*, Jose Hinojosa, Weijia Yao,
Juan Jimenez, Hector Garcia de Marina, *Member, IEEE*

Abstract—We propose a self-contained, resilient and fully distributed solution for locating the maximum of an unknown scalar field using a swarm of robots that travel at a constant speed. Unlike conventional reactive methods relying on gradient information, our methodology enables the swarm to determine an ascending direction so that it approaches the source with an arbitrary precision. Our source-seeking solution consists of three distributed algorithms running simultaneously in a slow-fast closed-loop system. The fastest algorithm provides the centroid-relative coordinates of the robots and the next slower one provides the ascending direction to be tracked. The tracking of the ascending direction by single integrators is instantaneous; however, in this paper we will also focus on 2D unicycle-like robots with a constant speed. The third algorithm, the slowest one since the speed of the robots can be chosen arbitrarily slow, is the individual control law for the unicycle to track the estimated ascending direction. We will show that the three distributed algorithms converge exponentially fast to their objectives, allowing for a feasible slow-fast closed-loop system. The robots are not constrained to any particular geometric formation, and we study both discrete and continuous distributions of robots. The *swarm shape* analysis reveals the resiliency of our approach as expected in robot swarms, i.e., by amassing robots we ensure the source-seeking functionality in the event of missing or misplaced individuals or even if the robot network splits in two or more disconnected subnetworks. In addition, we enhance the robustness of the algorithm by presenting conditions for *optimal* swarm shapes, ensuring that the ascending directions are aligned with to the field's gradient. We exploit such an analysis so that the swarm can adapt to unknown environments by morphing its shape and maneuvering while still following an ascending direction. We analyze our solution with robots as kinematic points in n -dimensional Euclidean spaces and extend the analysis to 2D unicycle-like robots with constant speeds.

I. INTRODUCTION

A. Motivation and aim

The ability to detect and surround sources of chemicals, pollution, and radio signals effectively with robot swarms can enable persistent missions in vast areas for environmental monitoring, search & rescue, and precision agriculture operations [1]–[5]. In particular, seeking the source of a scalar field can

be regarded as one fundamental task in swarm robotics [6], [7] where the resiliency of the robot swarm is expected, i.e., the swarm preserves its functionality against unexpected adverse conditions, unknown (possibly unmodeled) disturbances and the malfunctioning of robot individuals. However, formal guarantees on the performance of a solution while remaining feasible in practice, e.g., by fitting into realistic robot dynamics, communications, and scalability, are one of the great challenges in swarm robotics [6]–[8]. In this regard, we present and rigorously analyze a distributed source-seeking strategy for robot swarms, where the source is reached even if individuals go missing during the mission.

B. Overview of our source-seeking strategy

To facilitate a fair comparison with existing algorithms in the next subsection, we first outline the key features of our solution. Our strategy guarantees with sufficient conditions an ascending direction rather than the gradient in order to guide the centroid of the robot swarm to the source of a scalar field, i.e., all the individual robots estimate distributively and track a common ascending direction. Indeed, considering an ascending direction offers more flexibility to the robot swarm since there are multiple ascending directions instead of the single gradient direction. The algorithm does not require a specific formation or shape for the robot swarm; in fact, we will show how the computed ascending direction reacts to the relation between the swarm shape and the scalar field. This fact will be exploited to maneuver the robot swarm by morphing its shape while getting closer to the source simultaneously. The lack of a shape requirement allows the algorithm to maintain performance even if some robots are missing, as the resulting formation shape still follows an ascending direction.

The proposed mathematical formulation for computing the ascending direction enables the extension from discrete robot configurations to a continuous distribution of robots. Indeed, the analysis of the swarm shape and the density of the robot distribution within allows us to guarantee *optimal shapes* so that the calculated ascending direction is parallel to the actual gradient. Of course, the algorithm is implemented in discrete robots eventually; notwithstanding, the *continuous* results are fairly achieved with a density of robots sufficiently high, i.e., a swarm. We will show that the ascending direction can be calculated distributively based on a consensus algorithm. Finally, since robots need it for the ascending direction estimation, we analyze a distributed algorithm to estimate the swarm centroid.

The presented solution is fully compatible with single integrator robots, and with the restrictive but more realistic

Jesus Bautista, Jose Hinojosa, and H. Garcia de Marina are with the Department of Computer Engineering, Automation, and Robotics, and the Institute of Mathematics (IMAG) at the University of Granada, Spain. A. Acuaviva is with the School of Mathematical Sciences, University of Lancaster, United Kingdom. J. Jimenez is with the Department of Computer Architecture and Automation, Universidad Complutense de Madrid, Spain. Weijia Yao is with the School of Robotics, Hunan University. Corresponding author e-mail: hgdemarina@ugr.es. The work of H.G. de Marina is supported by the grant Ramon y Cajal RYC2020-030090-I from the Spanish Ministry of Science, and the ERC Starting Grant *iSwarm* 101076091. * Bautista and Acuaviva contributed equally as first authors in this publication.

unicycle (i.e., Dubins car model) robots with a constant speed. Indeed, inspired by the analysis on how unicycles can track guiding vector fields [9], [10], we show how a team of 2D unicycles travelling at a constant speed can track a vector field consisting of ascending directions, and how the centroid of the team gets arbitrarily close to the source eventually. The nature of our swarm algorithm is purely reactive to the field, and it does not need scouting or gathering prior information about the scalar field, and it does not consider a bounded map either. In that regards, our algorithm is mainly suited to work in scalar fields with only one maximum point and whose gradient and Hessian are bounded.

C. Existing solutions: comparisons and trade-offs

This subsection reviews the advantages and limitations of source-seeking algorithms commonly employed in the literature. We keep in mind that robot systems are tailored to specific missions and requirements, e.g., robot dynamics, sensing restrictions, traveled distance, or even prior knowledge of the scenario, i.e., it is fair to acknowledge that there is no better algorithm than others in every single metric regarding a source-seeking task.

The popular field-climbing methods focus on estimating the gradient, and possibly the Hessian as well, of an unknown scalar field. In [11], [12], the gradient estimation occurs in a distributed manner, where each robot calculates the different gradients at their positions. Since each local gradient is different, a common direction for the team is achieved through a distance-based formation controller that maintains the cohesion of the robot swarm. It is worth noting that this method fails when a subset of neighboring robots adopts a *degenerate* shape, e.g., a line in a 2D plane. In addition, the formation shape and following the gradient in [11], [12] are not fully compatible tasks and they disturb each other, affecting the mission performance. Alternatively, in [13], [14], the gradient and Hessian are estimated at the centroid of a circular formation consisting of unicycles. However, this methodology is relatively rigid due to its mandatory circular shape. Such a formation of unicycles is also presented in [15], where robots utilize relative heading measurements rather than relative position measurements. In contrast, our algorithm calculates an ascending direction instead of the gradient, allowing our robot team to enjoy greater flexibility concerning formation shapes while still offering formal guarantees for reaching the source. Finally, for gradient-following methods under known field assumptions, a pioneering work is established in [1].

Extremum seeking is another technique employed extensively as discussed in [16]–[18]. In these studies, robots, which could potentially be just one, with nonholonomic dynamics execute periodic motions to facilitate a gradient estimation. However, when multiple robots are involved, there is a necessity for the exchange of estimated parameters. Furthermore, the resulting robot trajectories are often characterized by long and tortuous paths with sharp turns. In contrast, our algorithm generates smoother trajectories suitable for robots such as fixed-wing drones.

All the algorithms above require communication among robots sharing the measured strength of the scalar field.

Nonetheless, the authors in [19] offer an elegant solution involving the principal component analysis of the field that requires no sharing of the field strength. However, the centroid of the swarm is still necessary and communication might be in order to estimate it. It is worth noting that in [19], the initial positions of the robots determine the (time-varying) formation during the mission, and it is not under control. In comparison, although our algorithm requires communication among robots due to the usage of a consensus algorithm, it is compatible with formation control laws, at least for single-integrators, so that it makes the trajectory of the robots more predictable.

Another family of source-seeking algorithms is information-based, which differs from the previously discussed algorithms, including our proposed one, as they are not purely reactive to the field. Information-based strategies can handle multiple sources but at the cost of requiring prior knowledge of the field, or at least they necessitate additional stages before seeking in order to estimate or scout the scalar field. However, the performance of these algorithms is more often supported by compelling experimental evidence rather than analytical proofs [20]–[22]. In connection with information-based algorithms, we conclude this review by briefly discussing a related problem, namely, the mobile-sensing coverage problem [23]–[25]. Algorithms addressing this problem are particularly effective at handling multiple sources simultaneously with a robot swarm. They primarily rely on partitioning the area using Voronoi cells. However, the performance comes at a higher cost compared to typical source-seeking solutions: individual robots require dense or continuous information about the scalar field within their corresponding Voronoi cell, and the area to be covered must be predetermined.

D. Extensions from our previous conference paper

Regarding the evolution from our conference work [26] to this journal paper, we address the following new points:

- We demonstrate a robot deployment strategy using degenerate formations, i.e., orthogonal line configurations, to estimate the gradient of the scalar field. We show that the key idea to estimate an ascending direction lies on the spatial variance of the robot deployment.
- The ascending direction can be computed distributively by just requiring a connected network.
- In order to provide a self-contained solution, we rigorously analyze a distributed algorithm that estimates the centroid of the robot swarm, assuming a shared, connected network. We also provide a corollary where all robots can localize themselves with respect to a designated robot.
- To address more realistic robot models, we rigorously analyze the compatibility of our methodology with teams of 2D unicycle robots travelling at a constant and equal speed. In particular, we show how to track the ascending direction with sufficient accuracy to ensure that the swarm's centroid can get arbitrarily close to the source.
- The three distributed algorithms (estimation of the centroid, ascending direction and its tracking) show exponential convergence to their individual objectives; therefore, facilitating their integration in a slow-fast closed-loop system.

E. Organization

The article is organized as follows. In Section II, we introduce notations, the considered robot dynamics and assumptions on the considered scalar field to formally state our source-seeking problem. We continue in Section III on how to calculate an ascending direction and how a *swarm* can be represented as a continuum distribution of robots. Also, in the same section, we analyze the observability of the gradient and the sensitivity of the ascending direction concerning the spatial shape of the swarm. We present the architecture of the source-seeking solution in Section IV. We first demonstrate the compatibility of our solution with single-integrator robots and a standard displacement-based formation control algorithm. Then, we provide a detailed analysis of two distributed algorithms: one for estimating the swarm's centroid and another for determining the ascending direction that needs to be tracked. In Section V, we rigorously present the tracking of the ascending direction by robots modeled as 2D unicycles travelling at constant speed, and how the exponential convergence of all the presented algorithms facilitates their simultaneous execution within a slow-fast closed-loop system. We validate our results in Section VI with simulations involving hundreds of robots. Finally, we end this article in Section VII with some conclusions.

II. PRELIMINARIES AND PROBLEM FORMULATION

A. Generic notation

Given a matrix $A \in \mathbb{R}^{p \times q}$, we define the operator $\bar{A} := A \otimes I_m \in \mathbb{R}^{pm \times qm}$, where \otimes denotes the Kronecker product and I_m is the identity matrix with dimension $m = \{2, 3\}$. We denote by $\mathbf{1}_p \in \mathbb{R}^p$ the all-one column vector; by $\|\cdot\|$, the standard Euclidean norm for vectors and the induced 2-norm for matrices; by A^\top the transpose of the vector/matrix A ; and by $|A|$ the determinant of A . The $+\pi/2$ rotation matrix is given by $E = \begin{bmatrix} 0 & -1 \\ 1 & 0 \end{bmatrix}$. Finally, $O(m)$ denotes the full orthogonal group (rotations and reflections), and the n -sphere is defined as $\mathbb{S}^n := \{x \in \mathbb{R}^{n+1} \mid \|x\| = 1\}$. In the case of the 1-sphere, we use the angular representation $\mathbb{S}^1 \simeq \mathbb{T}$, where $\mathbb{T} := (-\pi, \pi]$.

B. Graph Theory

Since our proposed source-seeking solution consists of distributed algorithms, we need to introduce some notions from Graph Theory [27] in order to precisely define the relationships between the robots. Consider a group of $N > m$ robots, then a *graph* $\mathcal{G} = (\mathcal{V}, \mathcal{E})$ consists of two non-empty sets: the node set $\mathcal{V} := \{1, \dots, N\}$ where each node i corresponds to the robot i , and the ordered edge set $\mathcal{E} \subseteq (\mathcal{V} \times \mathcal{V})$ defining the communications or sensing between pairs of different robots. For an arbitrary edge $\mathcal{E}_k = (\mathcal{E}_k^{\text{head}}, \mathcal{E}_k^{\text{tail}})$, we call its first and second element the *head* and the *tail* respectively. The set \mathcal{N}_i containing the neighbors of the node i is defined by $\mathcal{N}_i := \{j \in \mathcal{V} : (i, j) \in \mathcal{E}\}$.

We only deal with the special case of *undirected* graphs throughout the article, where all the edges \mathcal{E}_k are considered *bidirectional*, i.e., if $(i, j) \in \mathcal{E}$ then it implies that $(j, i) \in \mathcal{E}$. For an undirected graph, we choose only one of these two arbitrary directions between nodes i and j , so that we can

construct the *incidence matrix* $B \in \mathbb{R}^{|\mathcal{V}| \times |\mathcal{E}|}$ of \mathcal{G} as $b_{ik} = 1$ if $i = \mathcal{E}_k^{\text{tail}}$, -1 if $i = \mathcal{E}_k^{\text{head}}$ and 0 otherwise. For an undirected graph, the *Laplacian matrix* $L \in \mathbb{R}^{|\mathcal{V}| \times |\mathcal{V}|}$ [27, Chapter 6] can be calculated as $L = BB^\top$. If the graph \mathcal{G} is *connected* [27, Chapter 3], then the Laplacian matrix L has a single eigenvalue equal to zero, whose associated eigenvector is $\mathbf{1}_N$ since $B^\top \mathbf{1}_N = 0$; thus, L is positive semidefinite.

C. Robot dynamics and deployment

The position of the $i \in \mathcal{V}$ robot in the Euclidean space is represented by $p_i \in \mathbb{R}^m$. We define $p \in \mathbb{R}^{mN}$ as the stacked vector of the positions of all robots in the team, and the centroid of the team as $p_c := \frac{1}{N} \sum_{i=1}^N p_i$. Thus, we can write $p_i = p_c + x_i$, where $x_i \in \mathbb{R}^m$ for all $i \in \mathcal{V}$ represents the centroid-relative coordinates, describing how the robots are distributed around the centroid.

In this work, we consider both dynamics for the robots, the single integrator and the 2D unicycle with constant speed. The single integrator dynamics are modeled by

$$\dot{p}_i = u_i, \quad (1)$$

where $u_i \in \mathbb{R}^m$ is the control action, or guidance velocity in practice. The 2D unicycle model, assuming without loss of generality a constant speed of 1 in a convenient unit system, is given by

$$\begin{cases} \dot{p}_i = [\cos \alpha_i & \sin \alpha_i]^\top \\ \dot{\alpha}_i = \omega_i, \end{cases} \quad (2)$$

where $\omega_i \in \mathbb{R}$ is the angular velocity, serving as the control input that drives the robot's heading angle $\alpha_i \in \mathbb{T}$.

For a robot swarm, we define its spatial arrangement, referred to as *deployment*, as follows.

Definition 1. The *deployment* of a robot team is defined as the stacked vector $x := [x_1^\top \dots x_N^\top]^\top \in \mathbb{R}^{mN}$. We say that a deployment is not *degenerated* if all x_i 's span \mathbb{R}^m .

Therefore, a necessary condition for a deployment not being degenerated is that $N > m$. Additionally, a deployment is degenerated if and only if $\text{rank}(P(x)) < m$, where $P(x) := \frac{1}{N} \sum_{i=1}^N x_i x_i^\top$ is the covariance matrix of the deployment.

D. The scalar field and problem statement

The strength of a signal throughout the space can be described by a scalar field.

Definition 2. A *signal* is a scalar field $\sigma : \mathbb{R}^m \rightarrow \mathbb{R}^+$ which is class C^2 and all its partial derivatives up to second order are bounded uniformly. Also, σ has only one maximum at $p_\sigma \in \mathbb{R}^m$, i.e., the source of the signal, and its gradient at $a \in \mathbb{R}^m$ satisfies $\nabla \sigma(a) \neq 0 \iff a \neq p_\sigma$ and $\lim_{|a| \rightarrow \infty} \sigma(a) = 0$.

Our definition of signal encompasses numerous physical-world models, especially Gaussian distributed signals and signals that decay from the source following a power law $x^{-\alpha}$ (where $2 \leq \alpha \leq 3$) beyond a minimum distance x_{\min} from the origin [28]. Such signal strengths can represent the modulus of the electromagnetic field, the concentration of a contaminant, or heat radiation. In particular, quadratic scalar

fields are relevant in the physical world when considering the inverse of the power law x^{-2} or the logarithm of a Gaussian distribution.

In this paper, the gradient is defined as a column vector, i.e., $\nabla\sigma(\cdot) \in \mathbb{R}^m$, and according to our definition of a signal:

$$\|\nabla\sigma(a)\| \leq K \quad \text{and} \quad \|H_\sigma(a)\| \leq 2M, \forall a \in \mathbb{R}^m, \quad (3)$$

where $K, M \in \mathbb{R}^+$, and H_σ is the Hessian of the scalar field σ , i.e., $H_\sigma(a) \in \mathbb{R}^{m \times m}$.

Now, we are ready to define the source-seeking problem.

Problem 1 (Source-seeking). Given an unknown signal σ and a constant $\epsilon \in \mathbb{R}^+$, find control actions for (1) or (2) such that $\|p_c(t) - p_\sigma\| < \epsilon, \forall t \geq T$ for some finite time $T \in \mathbb{R}^+$.

III. ASCENDING DIRECTIONS FOR GENERIC DEPLOYMENTS

A. The ascending direction

Considering a generic (non-degenerated) deployment x , we will prove that

$$L_\sigma(p_c, x) := \frac{1}{ND^2} \sum_{i=1}^N \sigma(p_c + x_i) x_i \quad (4)$$

is an ascending direction at p_c whenever $p_c \neq p_\sigma$, where $D = \max_{1 \leq i \leq N} \|x_i\|$. Unlike prior works that focus on gradient estimation for non-degenerated deployments (e.g., equally angle-spaced circular formations [13]), the ascending direction here is not necessarily parallel to the gradient. This property relaxation provides key practical advantages, such as enabling swarm maneuvering through simple morphing of x or ensuring an ascending direction even in the presence of misplaced or missing robots with respect to a reference deployment.

Let us approximate $\sigma(p_c + x_i)$ in (4) to a two-term Taylor series for *small* $\|x_i\|$, i.e., $\sigma(p_c + x_i) \approx \sigma(p_c) + \nabla\sigma(p_c)^\top x_i$, so that $L_\sigma(p_c, x) \approx L_\sigma^0(p_c, x) + L_\sigma^1(p_c, x)$, where $L_\sigma^0(p_c, x) = \frac{1}{ND^2} \sum_{i=1}^N \sigma(p_c) x_i = 0$ since $\sum_{i=1}^N x_i = 0$, and

$$L_\sigma^1(p_c, x) = \frac{1}{ND^2} \sum_{i=1}^N (\nabla\sigma(p_c)^\top x_i) x_i. \quad (5)$$

Although the primary property of L_σ^1 lies in its direction, the factor $\frac{1}{ND^2}$ ensures that L_σ^1 shares the same physical units as the gradient. The direction of the vector L_σ^1 is particularly significant because, if x is non-degenerate, then it is an *always-ascending* direction, in the sense that no more conditions are necessary, towards the source p_σ at the centroid p_c .

Remark 1. While the robots compute L_σ as defined in (4), we introduce L_σ^1 in (5) for analytical purposes. This tractable approximation helps to reveal how the deployment geometry and scalar field properties influence the algorithm's behavior. Although L_σ^1 is not used in practice, we show in the following result that the error between L_σ and L_σ^1 is bounded, and for certain families of fields and deployments is actually zero. ◀

For the sake of completeness and to ensure a smooth reading flow, we present the key technical results, some of which have

been reworked for greater generality and improved coherence, from our conference work [26].

Lemma 1. ([26, Lemma 1]) $L_\sigma^1(p_c, x)$ is an always-ascending direction at p_c towards the maximum p_σ of the scalar field σ if the deployment x is non-degenerate and $p_c \neq p_\sigma$.

Proof. L_σ^1 is an always-ascending direction if and only if it satisfies $\nabla\sigma(p_c)^\top L_\sigma^1(p_c, x) > 0$, which is true since $\nabla\sigma(p_c)^\top L_\sigma^1(p_c, x) = \frac{1}{ND^2} \sum_{i=1}^N (\nabla\sigma(p_c)^\top x_i)^2$ is positive if the deployment x spans \mathbb{R}^m and $p_c \neq p_\sigma$. ◻

Lemma 1 motivates us to analyze how L_σ^1 (5) diverges from L_σ (4), the actual computed direction, concerning $\|x\|$.

Lemma 2. ([26, Lemma 2]) For a signal σ , a conservative divergence between $L_\sigma^1(p_c, x)$ and $L_\sigma(p_c, x)$ depends linearly on D , i.e.,

$$\|L_\sigma(p_c, x) - L_\sigma^1(p_c, x)\| \leq MD,$$

where M is the upper bound in (3).

Proof. From (4) and (5) and the Taylor series expansion, it follows that

$$\begin{aligned} \|L_\sigma - L_\sigma^1\| &= \frac{1}{ND^2} \left\| \sum_{i=1}^N (\sigma(p_c + x_i) - \sigma(p_c) - \nabla\sigma(p_c)^\top x_i) x_i \right\| \\ &\leq \frac{1}{ND^2} \sum_{i=1}^N M \|x_i\|^3 \leq MD. \end{aligned} \quad \square$$

If D is sufficiently small, then it is certain that L_σ is an ascending direction like L_σ^1 . However, how *small* D should be for generic signals and deployments depends on the maximum gradient and curvature/Hessian of the scalar field, already defined in (3). Considering a compact set $\mathcal{S} \subset \mathbb{R}^m$ with $p_\sigma \notin \mathcal{S}$, by the definition of σ and its bounded gradient, we know from Lemma 1 that $\nabla\sigma(p_c)^\top L_\sigma^1(p_c, x)$ is strictly positive if x is non-degenerate, thus it has a lower bound $F_\mathcal{S}(x) > 0$ that depends on the chosen deployment x . Therefore, defining $L_\sigma^e := L_\sigma - L_\sigma^1$ so that $\nabla\sigma(p_c)^\top L_\sigma = \nabla\sigma(p_c)^\top (L_\sigma^1 + L_\sigma^e)$, from Lemma 2 we have $\nabla\sigma(p_c)^\top L_\sigma \geq F_\mathcal{S}(x) - K_\mathcal{S}^{\max} M_\mathcal{S} D$, where $K_\mathcal{S}^{\max}$ and $M_\mathcal{S}$ are the maximum norms of the signal's gradient and Hessian in \mathcal{S} , respectively; thus, if

$$F_\mathcal{S}(x) - K_\mathcal{S}^{\max} M_\mathcal{S} D > 0, \quad (6)$$

then L_σ is an ascending direction in \mathcal{S} . Finding the lower bound $F_\mathcal{S}(x)$ numerically can be arduous, so we will provide a more handy expression after the next technical result.

Lemma 3. If the deployment x is non-degenerate, then

$$0 < \frac{\lambda_{\min}\{P(x)\}}{D^2} \leq \frac{\nabla\sigma(p_c)^\top L_\sigma^1(p_c, x)}{\|\nabla\sigma(p_c)\|^2} \leq \frac{\lambda_{\max}\{P(x)\}}{D^2},$$

where $\lambda_{\min}\{P(x)\}$ and $\lambda_{\max}\{P(x)\}$ are the minimum and maximum eigenvalues of $P(x)$, respectively.

Proof. First, the trivial case $\nabla\sigma(p_c) = 0$ satisfies the claim. In any other case, observe that $(\nabla\sigma(p_c)^\top x_i) x_i = (x_i x_i^\top) \nabla\sigma(p_c)$, so that $\nabla\sigma(p_c)^\top L_\sigma^1(p_c, x) = \frac{1}{D^2} \nabla\sigma(p_c)^\top P(x) \nabla\sigma(p_c)$ where $P(x)$ is symmetric and positive definite due to the non-degeneracy of x . Hence, applying the Rayleigh quotient bounds to $P(x)$ yields to the claim. ◻

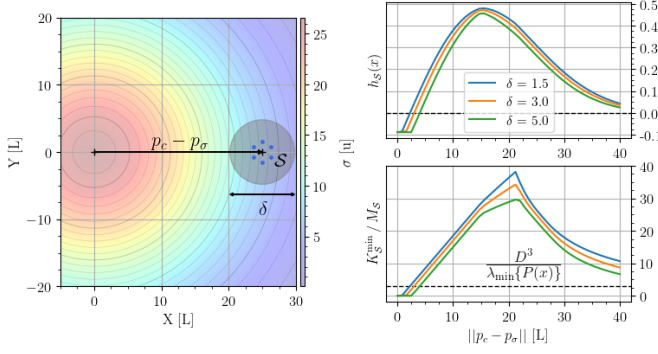


Fig. 1. Numerical illustration for Proposition 1. On the left, a radial scalar with field seven robots (blue dots) deployed at the vertices of a regular heptagon with $D = 0.75$. On the right, evaluation of the condition $h(x)$ in (7) and the ratio K_S^{\min}/M_S for circle sets S of different diameters δ (grey circle), relative to $\|p_c - p_\sigma\|$. The condition's lower bound is shown as a dashed black line.

Proposition 1. ([26, Proposition 1]) Let S be a compact set with $p_\sigma \notin S$, and every $p_i \in S$. Then if

$$h_S(x) := \frac{\lambda_{\min}\{P(x)\}}{D^2} K_S^{\min} - M_S D > 0, \quad (7)$$

where K_S^{\min} is the minimum norm of the gradient in the compact set S , then L_σ in (4) is an ascending direction at $p_c \in S$.

Proof. Given the lower bound for $\nabla\sigma(p_c)^\top L_\sigma^1(p_c, x)$ from Lemma 3, and the upper bound for $L_\sigma^e = L_\sigma - L_\sigma^1$ from Lemma 2, then we have that

$$\begin{aligned} \nabla\sigma(p_c)^\top L_\sigma(p_c, x) &= \nabla\sigma(p_c)^\top L_\sigma^1(p_c, x) + \nabla\sigma(p_c)^\top L_\sigma^e \\ &\geq h_S(x). \end{aligned} \quad (8)$$

Therefore, assuming $h_S(x) > 0$, then $L_\sigma(p_c, x)$, with every $p_i \in S$, is an ascending direction. \square

Remark 2. We note that the covariance matrix $P(x)$ is normalized by D^2 when verifying the condition in Proposition 1, which makes the effective dependency on D linear. This is consistent with the result of Lemma 2. \blacktriangleleft

Example 1. In Figure 1 we illustrate the result of Proposition 1 numerically. Given a symmetrical Gaussian signal with seven robots deployed at the corners of a regular heptagon with $D = 0.75$, we show for different balls S (centered at p_c) how depending on the distance to the source we can guarantee that L_σ is an ascending direction. \blacktriangle

Although the signal σ is unknown, Proposition 1 allows for the design of D based on expected scenarios. For instance, similarly as in Example 1, in the case of contaminant leakage, scientists can provide the expected values of M_S , K_S^{\max} , and K_S^{\min} within the patrolling area S . These values correspond to the maximum and minimum contamination thresholds at which the robot team must respond reliably. Furthermore, designing L_σ^1 to be parallel to the gradient $\nabla\sigma$ enhances the robustness of $\nabla\sigma^\top L_\sigma > 0$ with respect to D , as it allows for a larger deviation of L_σ from L_σ^1 , e.g., due to robots deviating from a reference deployment x . Thus, it is worthwhile to analyze which deployments best align L_σ^1 with the direction of $\nabla\sigma$. This is the focus of the following two subsections.

B. Symmetry Analysis in Discrete Deployments

In the following technical result, we show that for any deployment $x^{N\text{poly}}$ forming a regular polygon or polyhedron, L_σ^1 aligns with the gradient $\nabla\sigma(p_c)$.

Lemma 4. Consider the deployment $x^{N\text{poly}}$ forming a regular polygon or polyhedron, and $b \in \mathbb{R}^m$, then

$$\sum_{i=1}^N (b^\top x_i) x_i \propto b.$$

Proof. First, we have that $\sum_{i=1}^N (b^\top x_i) x_i = \sum_{i=1}^N (x_i x_i^\top) b = NP(x)b$; then, in order for this expression to be proportional to b , all diagonal elements of $P(x)$ must be equal and non-zero, and all off-diagonal elements must be zero. Since the symmetry group of an N -sided regular polygon is the dihedral group D_N , we can invoke Schur's Lemma to conclude that $P(x) \propto I_m$, i.e., $P(x)b \propto b$, which completes the proof. \square

The geometric interpretation of Lemma 4 is straightforward. When the deployment is centered at the origin and equally distributed alongside all the axes, e.g., the robots are at the vertices of a regular polygon, then the spatial spread is uniform in all directions, and $P(x) \propto I_m$. Furthermore, if the deployment is transformed by any matrix $R \in O(m)$, the new deployment $\tilde{x} = (I_N \otimes R)x$ yields $P(\tilde{x}) = RP(x)R^\top$. Since $P(x) \propto I_m$ it follows that $P(\tilde{x}) \propto I_m$ as well. Thus, the result in Lemma 4 holds regardless of the deployment's orientation relative to the coordinate axes. Note that we have arrived at the same conclusion as in [13], [14] but without the intensive usage of trigonometry for circular and spherical formations, as regular polygons and polyhedra are naturally inscribed in the circle and the sphere.

Remark 3. Using trigonometric calculations, one can show for $x = x^{N\text{poly}}$ that $P(x) = \frac{\rho^2}{2} I_m$, where $\rho > 0$ is the radius of the circumscribed circle/sphere. In this case, the bounds in Lemma 4 are tight, and we obtain $\nabla\sigma^\top L_\sigma^1 = \frac{\rho^2}{2D^2} \|\nabla\sigma\|^2$. \blacktriangleleft

We now analyze the sensitivity of $L_\sigma^1(p_c, x^{N\text{poly}})$ when the deployment is under an affine transformation, e.g., scaling, rotation, and shearing. The formal affine transformation is given by $(I_N \otimes A)x^{N\text{poly}}$ with $A \in \mathbb{R}^{m \times m}$ where A admits the Singular Value Decomposition (SVD) $A = U\Sigma V^\top$ describing a rotation, scaling, and another rotation.

Proposition 2. ([26, Proposition 2]) Consider the deployment $x^{N\text{poly}}$ forming a regular polygon or polyhedron, and the SVD $A = U\Sigma V^\top$, then

$$L_\sigma^1(p_c, (I_N \otimes A)x^{N\text{poly}}) \propto U\Sigma^2 U^\top r,$$

where $r \in \mathbb{S}^{m-1}$ is the unitary vector marking the direction of the gradient $\nabla\sigma(p_c)$.

Proof. Considering the change of coordinates $\tilde{r} = V\Sigma U^\top r$

$$\begin{aligned} L_\sigma^1(p_c, (I_N \otimes (U\Sigma V^\top))x^{N\text{poly}}) &\propto \sum_{i=1}^N (r^\top U\Sigma V^\top x_i) U\Sigma V^\top x_i \\ &\propto U\Sigma V^\top \sum_{i=1}^N (\tilde{r}^\top x_i) x_i \propto U\Sigma V^\top \tilde{r} = U\Sigma V^\top V\Sigma U^\top r = U\Sigma^2 U^\top r, \end{aligned}$$

where we have applied Lemma 4. \square

Note that $W = U\Sigma^2U^\top$ is the unitary decomposition of a positive definite matrix, and V is irrelevant, as shown in Lemma 4. Stretching the deployment $x^{N_{\text{poly}}}$ results in L_σ^1 following the direction $\Sigma_\xi^2 \nabla \sigma_\xi(p_c)$, where ξ denotes the *stretching axes*. Such a morphing assists with maneuvering the swarm while it gets closer to the source.

We proceed presenting an alternative application of Lemma 4, i.e., we can make L_σ^1 equal to half of the gradient by deploying two orthogonal segments of robots with identical covariance.

Proposition 3. *Consider an even number of robots N , divided in two degenerated and perpendicular 2D segment deployments, denoted by x_\parallel and x_\perp , each with $N_\parallel = N_\perp = N/2$ robots symmetrically distributed about their shared centroid. For both segments, within each semihalf, let robot $i = 1$ be the farthest from the centroid at a distance $a_1 \in \mathbb{R}^+$, and the rest $i \in \{2, \dots, \frac{N_\parallel}{2}\}$ at distances $0 \leq a_{i+1} < a_i$ such that $\sum_{i=2}^{\frac{N}{2}} a_i^2 = \frac{N}{4} a_1^2$. If N is an odd number, then place one robot at the centroid, e.g., $a_0 = 0$. Then, $\lim_{N_\parallel \rightarrow \infty} L_\sigma^1(p_c, x_\parallel) + \lim_{N_\perp \rightarrow \infty} L_\sigma^1(p_c, x_\perp) = \frac{1}{2} \nabla \sigma(p_c)$.*

Proof. We first note that a robot at $x_i = 0$ does not contribute at all; hence, since we require reflective symmetry around $x = 0$ we can assume that N_\parallel and N_\perp are even so that their halves are also integer numbers. Looking at (5), we have that

$$L_\sigma^1(p_c, x_\parallel) = \frac{\|\nabla \sigma(p_c)\| \cos(\theta_\parallel)}{N_\parallel a_1^2} 2 \sum_{i=1}^{\frac{N_\parallel}{2}} \begin{bmatrix} a_i^2 \\ 0 \end{bmatrix},$$

where $\theta_\parallel \in \mathbb{T}$ is the angle between $\nabla \sigma(p_c)$ and the direction of x_\parallel . Applying the condition $\sum_{i=2}^{\frac{N}{2}} a_i^2 = \frac{N}{4} a_1^2$ yields

$$\begin{aligned} L_\sigma^1(p_c, x_\parallel) &= \frac{2\|\nabla \sigma(p_c)\| \cos(\theta_\parallel)}{N_\parallel a_1^2} \begin{bmatrix} a_1^2 + \frac{N_\parallel}{4} a_1^2 & 0 \end{bmatrix}^\top \\ &= \frac{1}{2} \|\nabla \sigma(p_c)\| \cos(\theta_\parallel) \begin{bmatrix} \frac{4+N_\parallel}{N_\parallel} & 0 \end{bmatrix}^\top. \end{aligned}$$

Similarly, we can arrive at $L_\sigma^1(p_c, x_\perp) = \frac{1}{2} \|\nabla \sigma(p_c)\| \sin(\theta_\parallel) \begin{bmatrix} 0 & \frac{4+N_\perp}{N_\perp} \end{bmatrix}^\top$. Thus, we have that $\lim_{N_\parallel \rightarrow \infty} L_\sigma^1(p_c, x_\parallel) + \lim_{N_\perp \rightarrow \infty} L_\sigma^1(p_c, x_\perp) = \frac{\nabla \sigma(p_c)}{2}$. \square

The deployment's conditions required by Proposition 3 can be satisfied by a geometric series of the form $a_{i+1} = \alpha a_i$, $i \in \{1, \dots, (\frac{N_\parallel}{2} - 1)\}$, for some $0 < \alpha < 1$, and $a_{N_\parallel/2} = -\left(\sum_{i=2}^{\frac{N}{2}-1} a_i^2 - \frac{N}{4}\right) < a_1^2$. While the specific deployment pattern proposed in Proposition 3 is only a suggestion, it demonstrates that amassing robots makes more robust the parallel estimation of the gradient. For example, if few robots are missing or slightly misplaced, the variance of the deployment is less susceptible to change significantly, as illustrated in Figure 2.

Remark 4. Having a degenerated deployment x might make the gradient unobservable; nonetheless, in general, it is possible to estimate an ascending direction. \blacktriangleleft

The exploitation of symmetries does not stop with L_σ^1 . Indeed, focusing on the second-order term of the Taylor series of $\sigma(p)$ in L_σ as given in (4) we have the approximation

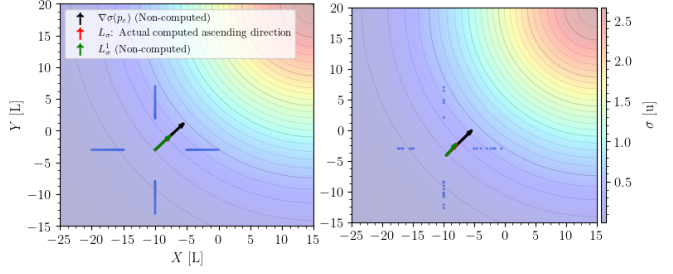


Fig. 2. Two perpendicular segment deployments following the distribution suggested in Proposition 3. On the left, we have a swarm of two segments with 40 robots each, and we can observe that the three directions L_σ , L_σ^1 and $\nabla \sigma(p_c)$ are almost parallel. On the right, we have removed 15 robots arbitrarily, and the direction of L_σ remains almost parallel to $\nabla \sigma(p_c)$. The vector L_σ^1 is the half of $\nabla \sigma(p_c)$ as predicted.

$L_\sigma(p_c, x) \approx L_\sigma^0(p_c, x) + L_\sigma^1(p_c, x) + L_\sigma^2(p_c, x)$, where

$$L_\sigma^2(p_c, x) := \frac{1}{ND^2} \sum_{i=1}^N \left(\frac{1}{2} x_i^\top H_\sigma(p_c) x_i \right) x_i.$$

It is straightforward to see that $L_\sigma^2(p_c, x) = 0$ for certain deployments, such as even distributions like $x^{N_{\text{poly}}}$. This observation has a positive impact for practical applications.

Proposition 4. *Consider an odd number of robots N , with a deployment x such that there exists a reflection matrix $R_r \in O(m)$ satisfying $R_r x_i = -x_j$, for every pair $i \neq j$, and a scalar field so that $\sigma(R_r p) = \sigma(p)$, then $L_\sigma^2(p_c, x) = 0$.*

Proof. Since $\sigma(R_r p) = \sigma(p)$, by expanding $\sigma(p)$ in a Taylor series, the Hessian satisfies the symmetry condition $R_r^\top H R_r = H$. Now, given that $R_r x_i = -x_j$, for every pair $i \neq j$, and that N is odd, $(x_i^\top H_\sigma x_i) x_i + (x_j^\top H_\sigma x_j) x_j = 0$ pairwise. Consequently, the statement follows. \square

In the case of a quadratic scalar field $\sigma(p) = b^\top p + \frac{1}{2} p^\top H p$, where $L_\sigma(p_c, x) = L_\sigma^1(p_c, x) + L_\sigma^2(p_c, x)$, Proposition 4 confirms that the second-order contribution cancels, yielding $L_\sigma(p_c, x) = L_\sigma^1(p_c, x)$. While simple, quadratic scalar fields has a direct relation with signal models that are very present in the physical world, such as the logarithm of Gaussian fields or the inverse of $r^{1/2}$ laws.

C. Symmetry Analysis in Continuous Robot Distributions

Looking at the definition of L_σ in (4), it is clear that we can apply the superposition of many, potentially infinite, deployments. This naturally leads to the concept of a *continuous* deployment, where we consider the limit as $N \rightarrow \infty$ over a prescribed region. In this regime, the finite sum in (4) is replaced by an integral, following the Riemann approximation of a definite integral, with a continuous robot density function. To ensure dimensional consistency, the term ND^2 in (4) is replaced by either $A = \iint_{\mathcal{A}} \rho(X, Y) dX dY$ or $V = \iiint_{\mathcal{V}} \rho(X, Y, Z) dX dY dZ$, where \mathcal{A}/\mathcal{V} is the corresponding surface/volume within the perimeter delimited by x , and $\rho: \mathcal{D} \rightarrow \mathbb{R}^+$, with $\mathcal{D} = \mathcal{A}$ or \mathcal{V} , is a normalized (robot) density function. Nonetheless, note that A and V are not essential for our algorithm, as we are only interested in the *direction* of the

ascending direction, not its magnitude. For clarity in notation, we denote x_i^X and x_i^Y simply as X and Y , respectively. Then, focusing on the 2D case, for a swarm distributed according to a density function $\rho(X, Y)$ over a generic surface \mathcal{A} , the always-ascending direction can be calculated as

$$\begin{aligned} L_\sigma^1(p_c, x) &= \frac{\|\nabla\sigma(p_c)\|}{A} \iint_{\mathcal{A}} \rho(X, Y) \begin{pmatrix} \cos(\theta) \\ \sin(\theta) \end{pmatrix}^\top \begin{bmatrix} X \\ Y \end{bmatrix} \begin{bmatrix} X \\ Y \end{bmatrix} dXdY \\ &= \frac{\|\nabla\sigma(p_c)\|}{A} \iint_{\mathcal{A}} \rho(X, Y) \begin{bmatrix} X^2 \cos(\theta) + XY \sin(\theta) \\ Y^2 \sin(\theta) + XY \cos(\theta) \end{bmatrix} dXdY, \end{aligned} \quad (9)$$

where $\theta \in \mathbb{T}$ is the angle between $\nabla\sigma(p_c)$ and the X -axis.

Adopting this continuum perspective, we now demonstrate in the next result that not only regular polygon/polyhedron deployments x^{Npoly} , but also a broader class of deployments exhibiting certain symmetries ensure that L_σ^1 aligns with the gradient $\nabla\sigma(p_c)$, like those in Figure 3.

Proposition 5. ([26, Proposition 3]) *Consider a signal σ , a continuous deployment x with robot density function $\rho(X, Y)$ within an area \mathcal{A} , and a Cartesian coordinate system $(X - Y)$ with origin at the centroid of the deployment p_c . The direction of $L_\sigma^1(p_c, x)$ is parallel to the gradient $\nabla\sigma(p_c)$ if $\rho(X, Y)$ and \mathcal{A} hold the following symmetries:*

- S0) *The robot density function $\rho(X, Y)$ has reflection symmetry (even function) concerning at least one of the axes $(X - Y)$, e.g., $\rho(X, Y) = \rho(-X, Y)$.*
- S1) *The surface \mathcal{A} has reflection symmetry concerning the same axes as in S0.*
- S2) *For each quadrant of $(X - Y)$, the robot density function $\rho(X, Y)$ has reflection symmetry concerning the bisector of the quadrant.*
- S3) *The surface \mathcal{A} has reflection symmetry concerning the same axes as in S2.*

Proof. To ensure that L_σ^1 aligns with the gradient $\nabla\sigma(p_c)$, looking at (9), it is sufficient to satisfy $\iint_{\mathcal{A}} \rho(X, Y)XY dXdY = 0$ and $\iint_{\mathcal{A}} \rho(X, Y)(X^2 - Y^2) dXdY = 0$.

For the first condition, we assume without loss of generality that the reflection symmetry is on the Y axis, and the symmetric integration limits for the horizontal axis as in Figure 4(a). First, if $\alpha(X)$ and $\beta(X)$ are both even functions as illustrated in Figure 4(a), let us show that

$$\begin{aligned} \iint_{\mathcal{A}} \rho(X, Y)XY dXdY &= \int_{-t_\beta}^{t_\beta} \int_0^{\beta(X)} \rho(X, Y)XY dXdY + \int_{-t_\alpha}^{t_\alpha} \int_{\alpha(X)}^0 \rho(X, Y)XY dXdY \\ &= \int_{-t_\beta}^{t_\beta} XF(X, \beta(X)) dX - \int_{-t_\alpha}^{t_\alpha} XF(X, \alpha(X)) dX = 0, \end{aligned} \quad (10)$$

where $F(X, Y) = \int \rho(X, Y)Y dY$. Given an arbitrary even function $f(X)$ and considering that $\rho(X, Y) = \rho(-X, Y)$, i.e., $F(X, Y) = F(-X, Y)$, then $F(X, Y) = F(X, f(X)) = F(-X, f(-X)) = F(X, -Y)$. Consequently, both integrals in (10) are zero considering symmetries S0 and S1.

For the second condition, we divide \mathcal{A} into four parts for each quadrant, as shown in Figure 4(b), so that

$$\iint_{\mathcal{A}} \rho(X, Y)(X^2 - Y^2) dXdY = \sum_{i=1}^4 \iint_{\mathcal{A}_i} \rho(X, Y)(X^2 - Y^2) dXdY,$$

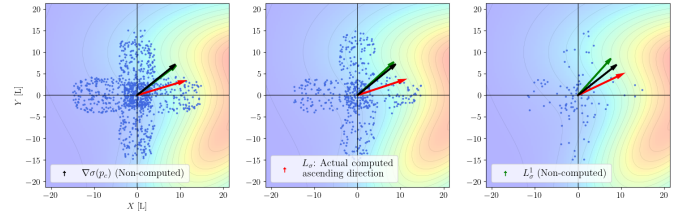


Fig. 3. On the left, a swarm of 1000 robots satisfying all the symmetries from Proposition 5. For the three figures, the black arrows are the gradient $\nabla\sigma$, the green arrows are L_σ^1 , and the red arrows are the direction L_σ computed by the robots. Arrows are normalized for representation purposes as we focus only on their direction. As we get far from *the continuum*, with 500 and 100 robots on the middle and right figures, there is no guarantee that L_σ^1 is parallel to the gradient $\nabla\sigma$.

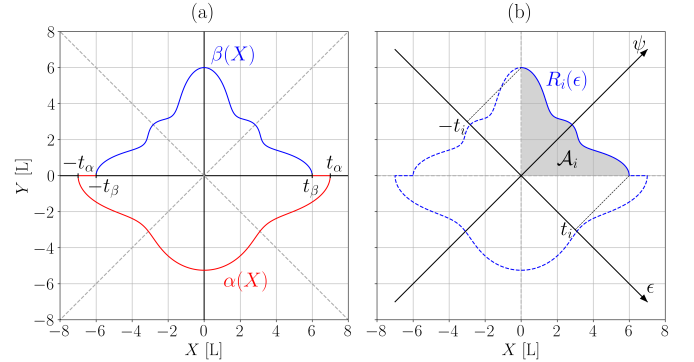


Fig. 4. Illustration of the symmetries S1 and S3 for the surface \mathcal{A} on the left and right respectively, to design $L_\sigma^1(p_c, x)$ parallel to $\nabla\sigma(p_c)$.

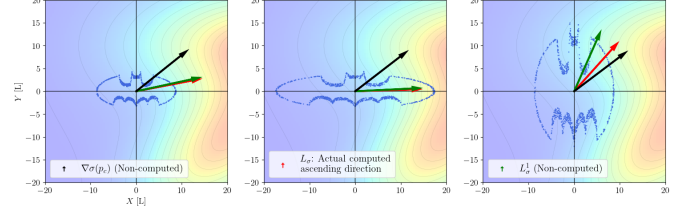


Fig. 5. On the left, a swarm of 1000 robots satisfying only the symmetries S0 and S1 from Proposition 5. The arrows have the same meaning as in Figure 3. The modification of the variances of $\rho(X, Y)$, e.g., by stretching the swarm shape, stretches L_σ^1 and L_σ accordingly.

where \mathcal{A}_i is the area of the quadrant $i \in \{1, 2, 3, 4\}$. From the symmetry exhibited by $X^2 - Y^2$ we propose the following change of variables $g(\epsilon, \psi) = (\psi + \epsilon, \psi - \epsilon)/\sqrt{2}$, which is equivalent to a rotation of $-\pi/4$ radians for the $(X - Y)$ axes. Since $\int_{\mathcal{A}} f(x, y) = \int_{\mathcal{B}} (f \circ g) |J_g|$, where $|J_g| = |\begin{bmatrix} \nabla g_1 & \nabla g_2 \end{bmatrix}^\top| = \sqrt{2}$, we have

$$\begin{aligned} \iint_{\mathcal{A}_i} \rho(X, Y)(X^2 - Y^2) dXdY &= 2\sqrt{2} \iint_{\mathcal{B}_i} \rho(\epsilon, \psi) \epsilon \psi d\epsilon d\psi \\ &= 2\sqrt{2} \int_{-t_i}^{t_i} \int_{|\epsilon|}^{R_i(\epsilon)} \rho(\epsilon, \psi) \epsilon \psi d\epsilon d\psi = 2\sqrt{2} \int_{-t_i}^{t_i} \epsilon [F(\epsilon, R_i(\epsilon)) - F(\epsilon, |\epsilon|)] d\epsilon, \end{aligned}$$

which is zero if $R_i(\epsilon) = R_i(-\epsilon)$ for all quadrants since $|\epsilon|$ is an even function. Such condition is satisfied if $\alpha(X)$ and $\beta(X)$ have reflection symmetry concerning the bisector of the two lower and upper quadrants respectively (S2 and S3), as illustrated in Figure 4(b). Thus, the statement follows. \square

When only S0 and S1 are satisfied, focusing on $\rho(X, Y)$ and its variances $\text{VAR}_A[X] \neq \text{VAR}_A[Y]$ yields

$$L_\sigma^1(p_c, x) = \frac{\|\nabla\sigma(p_c)\|}{A} \begin{bmatrix} \text{VAR}_A[X]r^X \\ \text{VAR}_A[Y]r^Y \end{bmatrix},$$

where the relation between variances *maneuvers* the swarm while getting closer to the source, as it is shown in Figure 5. Recall that $r \in \mathbb{S}^{m-1}$ denotes the unit vector indicating the direction of the gradient $\nabla\sigma(p_c)$.

D. Source seeking with single integrator robots

The following theorem shows that $L_\sigma(p_c(t), x)$ can guide the centroid of a robot swarm of single integrators to solve Problem 1 effectively.

Theorem 1 (Theorem 1 [26]). *Consider the signal σ as defined in Definition 2 and a swarm of N robots with dynamics (1). Assume that the initial deployment $x(0)$ is non-degenerate; then*

$$\begin{cases} \dot{p}_i(t) &= \frac{L_\sigma(p_c(t), x(t))}{\|L_\sigma(p_c(t), x(t))\|} \\ p_i(0) &= p_c + x_i(0), \quad p_c \neq p_\sigma \end{cases}, \forall i \in \{1, \dots, N\}, \quad (11)$$

is a solution to Problem 1 given the conditions of Proposition 1 for an annulus shell \mathcal{S} around p_σ .

Proof. We first consider the dynamics of the following system

$$\begin{cases} \dot{p}_i(t) &= L_\sigma^1(p_c(t), x(t)) \\ p_i(0) &= p_c + x_i^*, \quad p_c \neq p_\sigma \end{cases}, \forall i \in \{1, \dots, N\}, \quad (12)$$

and then we continue to analyse the system (11) in the statement. Let us consider the function $\sigma(p_c(t))$ with a positive maximum at p_σ , and without loss of generality, let us set p_σ at the origin so that $\sigma(p) \rightarrow \sup\{\sigma\} = \sigma(0)$ as $\|p\| \rightarrow 0$, and $\sigma(p) \rightarrow 0$ as $\|p\| \rightarrow \infty$. Because of Definition 2, $\sigma(p)$ does not have any local maxima or minima, but only the global maximum $\sup\{\sigma\} = \sigma(0)$. The dynamics of $\sigma(p_c(t))$ under (12) is:

$$\dot{\sigma}(p_c(t)) = \nabla\sigma(p_c)^\top \dot{p}_c(t) = \nabla\sigma(p_c)^\top L_\sigma^1(p_c(t), x(t)) \geq 0,$$

since $x(t)$ is not degenerated for all t , then the equality holds if and only if $p_c = p_\sigma$ because of Lemma 1.

Let us consider the Lyapunov function $V = (\sigma(p_c(t)) - \sigma(0))^2/2$, and calculating the time derivative with respect to (12), we have

$$\begin{aligned} \dot{V}(t) &= (\sigma(p_c(t)) - \sigma(0)) \nabla\sigma^\top(p_c(t)) \dot{p}_c(t) \\ &= \underbrace{(\sigma(p_c(t)) - \sigma(0)) \nabla\sigma^\top(p_c(t)) L_\sigma^1(p_c(t), x(t))}_{W(t)} \leq 0. \end{aligned}$$

At this point, we can invoke LaSalle's invariance principle to conclude that $W(t) \rightarrow 0$ as $t \rightarrow \infty$; or equivalently $\lim_{t \rightarrow \infty} p_c(t) = p_\sigma = 0$ since we recall that $x(t)$ is not degenerate. Therefore, given an $\epsilon > 0$, there is always a time $T^* > 0$, such that $\|p_c(t) - p_\sigma\| < \epsilon, \forall t > T^*$, as required to solve the source-seeking Problem 1.

Let us focus now on the system (11). We first know that $\frac{L_\sigma(p_c(t), x(t))}{\|L_\sigma(p_c(t), x(t))\|}$ is well defined in \mathcal{S} if $x(t)$ is not degenerate. Let us consider the annulus shell \mathcal{S} centered at p_σ and with radii $\epsilon^+ > \epsilon_- > 0$, then, according to Proposition 1, there

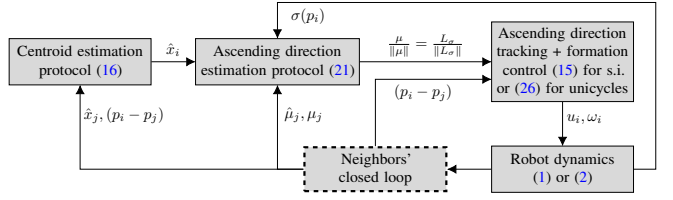


Fig. 6. Closed-loop system of an individual robot showing all the algorithms and inputs/outputs involved in the proposed source-seeking solution. The exponential convergence of the three blocks on top facilitates their interconnection in a slow-fast fashion. All (neighboring) robots run the same closed-loop system represented as a dashed block, and note how their (relative and absolute) positions are also in closed-loop; this is represented by the arrow going from "Robot dynamics" to "Neighbors' close loop" block.

exists $D^*(\epsilon^+, \epsilon_-)$ such that if $D \leq D^*$ the trajectory of $p_c(t)$ under the dynamics (11) is an ascending one so that we can apply the same arguments as for the system (11) and solve the source-seeking Problem 1 where $\epsilon = \epsilon_-$ and the initial condition must satisfy $\|p_c(0)\| \leq \epsilon^+$. \square

IV. DISTRIBUTED ARCHITECTURE OF THE PROPOSED SOURCE-SEEKING SYSTEM

So far, our methodology would require a central robot which collects all the $\sigma(p_c + x_i)x_i$ and computes L_σ as in (4); meaning that the entire robot swarm becomes non-operational if such computing robot serving as a nexus disappears. While assigning backup computing robots could be a solution, an alternative approach is to estimate all kind of required information distributively. The main idea is to enhance further the resilience of the robot swarm with a distributed architecture with no leaders and where individuals can join and leave the swarm in the middle of the mission. In order to provide a self-contained and distributed source-seeking solution, we show the following items in the upcoming subsections. Firstly, the compatibility of the source-seeking solution for single-integrator robots with a displacement-based formation controller. Secondly, the distributed estimation of the swarm centroid, i.e., each robot estimates its corresponding x_i in (4). This estimator is based on the *dual* version of the above formation controller. Lastly, the distributed calculation of the ascending direction (4).

We illustrate the closed-loop system architecture in Figure 6, where for single-integrator robots, the ascending-direction tracking occurs *instantaneously*. The tracking controller for the 2D unicycle will be presented in the upcoming Section V. We will see that the exponential convergence of each algorithm facilitates a slow-fast system interconnection, with centroid estimation being the fastest, and tracking being the slowest, since the constant speed for the robots can be set arbitrarily.

A. Compatibility with a displacement-based formation control

We briefly discuss how certain properties of a standard displacement-based formation controller can be leveraged with our source-seeking algorithm, particularly for single integrator dynamics. In addition, this briefing will help us introduce later the centroid estimator as a *dual* algorithm of the displacement-based formation controller.

As shown in Lemma 4, the computation of the ascending direction L_σ can be assisted with a convenient robot deployment x . If robots can measure or determine their relative positions, then the following control action for the single-integrator (1)

$$u_f^i = -k_f \sum_{j \in \mathcal{N}_i} (p_i - p_j) - (p_i^* - p_j^*), \forall i \in \mathcal{V}, \quad (13)$$

where $k_f \in \mathbb{R}^+$, drives all robots to their desired relative positions $(p_i^* - p_j^*)$ [29], and the compact form of (13) can be written as

$$u_f = -k_f \bar{L}(p - p^*), \quad (14)$$

where $u_f \in \mathbb{R}^{mN}$ is the stacked vector of control actions u_f^i and p^* is the desired deployment with respect to an arbitrary fixed reference frame, and L is the Laplacian matrix L . Note that the robots will not converge to the actual p^* , but to a point $p \in \mathcal{P} := \{p : p = p^* + (\mathbf{1}_N \otimes c), c \in \mathbb{R}^m\}$; i.e., what is important is that $\lim_{t \rightarrow \infty} p(t) \in \mathcal{P}$ has the required *shape*. In fact, if the desired shape p^* is written with respect to p_c , then $\lim_{t \rightarrow \infty} x(t) = p^*$ exponentially fast [30]. In particular, the vector $\mathbf{1}_N$ spans the kernel space of L ; therefore, having all the robots following the common velocity $\frac{L_\sigma}{\|L_\sigma\|}$, in addition to u_f , will not interfere with the formation control action, i.e., $\bar{L}(\mathbf{1}_N \otimes \frac{L_\sigma}{\|L_\sigma\|}) = 0$. In fact, u_f keeps the centroid of x invariant since $\sum_{i=1}^N u_f^i = 0$ due to $\mathbf{1}_N^\top L = \mathbf{1}_N^\top B B^\top = 0$ because $B^\top \mathbf{1}_N = 0$. Hence, we propose for the single-integrator robots (1) the following control action presented in compact form

$$u = \left(\mathbf{1}_N \otimes \frac{L_\sigma}{\|L_\sigma\|} \right) + u_f, \quad (15)$$

whose analysis to solve Problem 1 is similar to the Theorem 1, since u_f can be seen as a perturbation that vanishes exponentially fast.

B. Distributed estimation of the centroid

We continue with the algorithm that estimates the necessary centroid-relative coordinates x_i distributively. The proposed algorithm emerges from a collection of well-established results from formation control. In particular, the formation control problem has its dual in the relative localization problem [29], [31]. We first note that in (13) the *software* term $(p_i^* - p_j^*)$ defining the desired deployment is fixed, while the *hardware* term associated with the robot measurements $(p_i - p_j)$ is dynamic, i.e., the formation control action u_f^i actuates over the velocities of the robots \dot{p}_i . Now, consider the *dual dynamics* of (13)

$$\frac{d}{dt} \hat{x}_i(t) = - \sum_{j \in \mathcal{N}_i} \left((\hat{x}_i(t) - \hat{x}_j(t)) - (x_i - x_j) \right), \forall i \in \mathcal{V}, \quad (16)$$

where the network topology can be the same as before in (13) or (14), but now the fixed term is the *hardware* measurement $(x_i - x_j)$, which is equivalent to the relative position $(p_i - p_j)$, and the dynamic term is the *software* estimation $\hat{x}_i \in \mathbb{R}^m$, i.e., the estimation of the position of the centroid from the robot i . Note that since \hat{x}_j is a software value, then it needs to be communicated to robot i for all $(i, j) \in \mathcal{E}$. In practice,

the relative position between agents can be set to evolve slowly enough by adjusting the low-enough ratio between the (independent) constant speed of the robots and the running frequency (in discrete time) of (16). Moreover, the tracking of a time-varying signal by a consensus-based algorithm can also be improved by a collection of techniques presented in [32].

Proposition 6. *The estimation $\hat{x}_i(t)$ in (16) converges exponentially fast to the actual x_i as $t \rightarrow \infty$ if and only if $\sum_{i=1}^N \hat{x}_i(0) = 0$.*

Proof. We first recall that the considered type of graph for the following results is undirected and connected.

Let us write the compact form of (16) as

$$\begin{aligned} \frac{d}{dt} \hat{x}(t) &= -\bar{L} \hat{x}(t) + \bar{L} x \\ \frac{d}{dt} \hat{x}(t) + \bar{L} \hat{x}(t) &= \bar{B} z, \end{aligned} \quad (17)$$

where here L is the Laplacian matrix L again so that $z = \bar{B}^\top x = \bar{B}^\top p \in \mathbb{R}^{m|\mathcal{E}|}$ is the stacked vector of relative positions $(x_i - x_j) = (p_i - p_j), (i, j) \in \mathcal{E}$. We note that the dynamics of $\sum_{i=1}^N \hat{x}_i(t)$ are stationary, i.e., $\sum_{i=1}^N \frac{d}{dt} \hat{x}_i(t) = 0$ since

$$\mathbf{1}_{mN}^\top (-\bar{L} \hat{x}(t) + \bar{L} x) = 0, \quad (18)$$

in view of $L = B B^\top$ and $B^\top \mathbf{1}_N = 0$. Hence, if $\sum_{i=1}^N \hat{x}_i(0) = 0$, the centroid or average of $\hat{x}(t)$ will remain at zero $\forall t$. Note that this is a sufficient and also necessary condition for the invariance of the centroid of $\hat{x}(t)$ since $\mathbf{1}_N^\top$ is the only left eigenvector of L associated with its single zero eigenvalue. We also know that the eventual trajectory $\hat{x}^h(t)$ of the homogeneous part of the differential equation (17) is given by

$$\lim_{t \rightarrow \infty} \hat{x}^h(t) = \mathbf{1}_N \otimes c_1, \quad (19)$$

since $\mathbf{1}_N$ is the eigenvector associated with the single eigenvalue zero of L , $c_1 \in \mathbb{R}^m$ is up to the initial condition $\hat{x}(0)$, and the rest of terms of $\hat{x}^h(t)$ vanish exponentially fast since L is positive semidefinite. In fact, we know that, $c_1 = \frac{1}{N} \left(\sum_{i=1}^N \hat{x}_i(0) \right)$ for the homogeneous equation alone since it is a first-order consensus protocol [27]. However, this value for c_1 is not necessarily relevant for our analysis, since we have now a *forcing* term in (17) for a particular solution.

We can check that $\hat{x}^p = x + (\mathbf{1}_N \otimes c_2)$ is a family of particular solutions for (17), where $c_2 \in \mathbb{R}^m$; thus,

$$\lim_{t \rightarrow \infty} \hat{x}(t) = \left(\mathbf{1}_N \otimes (c_1 + c_2) \right) + x.$$

However, since the centroid of x is zero by definition, and the centroid of $\hat{x}(0)$ is assumed to be zero and it is invariant because of (18), it must be true that $c_1 + c_2 = 0$, i.e., x and $\hat{x}(t)$ share the same frame of coordinates; therefore, $\lim_{t \rightarrow \infty} \hat{x}(t) = x$, and it must happen exponentially fast as in a first order consensus protocol [27], [30]. \square

Remark 5. The condition $\sum_{i=1}^N \hat{x}_i(0) = 0$ can be satisfied by setting all the initial software values $\hat{x}_i(0) = 0$. \blacktriangleleft

The result of Proposition 6 can also be used to estimate the relative positions of two non-neighboring robots, or more generally, to localize all the robots with respect to a chosen

one. For example, once robot k estimates its centroid-relative coordinate x_k , we can initialize a new estimation network by setting $\sum_{i=1}^N \hat{x}_i(0) = -x_k$. In particular, robot k assigns $\hat{x}_k(0) = -x_k$, while the rest of the robots set their initial conditions to zero; thus $\lim_{t \rightarrow \infty} \hat{x}(t) = x - (\mathbf{1}_N \otimes x_k)$. We summarize this derivation with the following corollary.

Corollary 1. *The estimations \hat{x}_i in (16) converge exponentially fast to the relative positions $(p_i - p_k)$ as $t \rightarrow \infty$ if and only if $\sum_i^N \hat{x}_i(0) = -x_k$, where $k \in \mathcal{V}$.*

C. Distributed calculation of the ascending direction

As we have seen in (15), so far for single-integrator robots, the swarm can track the direction of L_σ . In this subsection, we are going to show that the direction of the vector L_σ as in (4) can be estimated with a consensus algorithm distributively. We first note that N and D^2 are not necessary to know the direction of L_σ ; therefore if we define

$$\mu_c(t) := \frac{1}{N} \sum_{i=1}^N \mu_i(t) = \frac{1}{N} \sum_{i=1}^N \sigma(p_c(t) + x_i(t))x_i(t), \quad (20)$$

then we have that $\frac{L_\sigma}{\|L_\sigma\|} = \frac{\mu_c}{\|\mu_c\|}$, i.e., the signals $\mu_c(t)$ and $L_\sigma(t)$ point at the same direction. Hence, if we set $\mu_i(0) = \sigma(p_c(0) + x_i(0))x_i(0)$, we have that $\lim_{t \rightarrow \infty} \mu_i(t) \rightarrow \mu_c(0)$ exponentially fast if a connected network within the robot swarm follows the consensus protocol

$$\begin{cases} \dot{\mu}_i(t) &= \sum_{j \in \mathcal{N}_i} (\mu_j(t) - \mu_i(t)) \\ \mu_i(0) &= \sigma(p_c(0) + x_i(0))x_i(0) \end{cases}, \quad \forall i \in \mathcal{V}. \quad (21)$$

However, the protocol (21) cannot run without resets each time suitable values of $\sigma(p_i)$ and \hat{x}_i are available for the whole network; moreover, the resulting ascending direction to feed the tracking controller has to be refreshed after an almost asymptotic value of $\mu_i(t) \rightarrow \mu_c(0)$ has been reached.

In order to have a dynamic protocol for the estimation of $\mu_c(t)$ that does not need to be reset, we are going to leverage Proposition 6, i.e., taking the dual dynamics of (13) where we will update a software value $\hat{\mu}(t)$ via hardware measurements $\mu_i(t)$ with the following protocol

$$\begin{cases} \frac{d}{dt} \hat{\mu}_i(t) &= -\sum_{j \in \mathcal{N}_i} ((\hat{\mu}_i(t) - \hat{\mu}_j(t)) - (\mu_i - \mu_j)) \\ \hat{\mu}_i(0) &= 0, \quad \forall i \in \mathcal{V}. \end{cases} \quad (22)$$

Note that the quantities $\mu_j, \hat{\mu}_j, j \in \mathcal{N}_i$ need to be shared with robot i .

Proposition 7. *Consider all robots are stopped, i.e., $\dot{p} = 0$; then, from the estimator (22) we have that $\mu_i - \lim_{t \rightarrow \infty} \hat{\mu}_i(t) = \mu_c$ exponentially fast, with μ_c as in (20).*

Proof. Since all robots are stopped, then all the readings $\sigma(p_i(t))$ and all the relative positions $(p_i(t) - p_j(t))$ are constant; hence all $\mu_i(t)$ are constant and thus $\mu_c(t)$ is also constant. Having the dynamics (22), we can conclude that $\lim_{t \rightarrow \infty} \hat{\mu}_i(t) = \mu_i - \mu_c$ from Proposition 6. \square

D. Slow-fast closed-loop system

Indeed, the signal $\mu_c(t)$ will be time-varying in practice, and as with protocol (16) we can consider techniques in [32] to track a dynamic signal to improve Proposition 7. Nonetheless, for the sake of conciseness we are going to consider the following two assumptions:

- The (independent) robots' speed are slow enough; hence, all the signal readings $\sigma(p_i)$ and all the relative positions $(p_i - p_j)$ evolve slowly.
- The dynamics of the centroid estimator (16) are much faster than the dynamics of (22) for the estimation of μ .

Having these two requirements in mind, we interconnect (16), (22), and (15), and construct the following slow-fast closed-loop system, as in Figure 6, for the single-integrator robots

$$\begin{cases} \epsilon_x \frac{d}{dt} \hat{x}_i(t) &= -\sum_{j \in \mathcal{N}_i} ((\hat{x}_i(t) - \hat{x}_j(t)) - (x_i(t) - x_j(t))) \\ \epsilon_\mu \frac{d}{dt} \hat{\mu}_i(t) &= -\sum_{j \in \mathcal{N}_i} ((\hat{\mu}_i(t) - \hat{\mu}_j(t)) - (\mu_i(t) - \mu_j(t))) \\ \frac{d}{dt} p_i &= \frac{\mu_c^i(t)}{\|\mu_c(t)\|} - k_f \sum_{j \in \mathcal{N}_i} (p_i(t) - p_j(t)) - (p_d^i - p_d^j) \\ \mu_i(t) &= \sigma(p_i(t)) \hat{x}_i(t) \\ \mu_c^i(t) &= \mu_i(t) - \hat{\mu}_i(t), \quad \text{for every } i \in \mathcal{V}, \\ \hat{x}_i(0) &= 0 \\ \hat{\mu}_i(0) &= 0 \end{cases} \quad (23)$$

where the measurements are the readings of the scalar field $\sigma(p_i(t))$ and the relative positions $(x_i(t) - x_j(t))$, $(i, j) \in \mathcal{E}$, the desired deployment is $x_d = p_d - p_c$, with $x_d \in \mathbb{R}^{mN}$. Now, let us argue that for sufficiently small $\epsilon_x, \epsilon_\mu < 1$, the tracking of the ascending direction is stable in the sense that $\dot{p}_c(t) \rightarrow R(\delta) \frac{\mu_c(t)}{\|\mu_c(t)\|}$ exponentially fast until the gradient starts vanishing close to the source p_σ as required in Problem 1, with $R(\delta(t)) \in \text{SO}(m)$ and $\|\delta(t)\| \leq \epsilon_\delta$ small enough so $\dot{p}_c(t)$ stays as an ascending direction when $p_c \neq p_\sigma$. We note that the asymptotic value of $\mu_c^i \neq 0$ in general, i.e., when the centroid is far from the source. For example, in order to avoid a possible singularity, the motion of the agents in system (23) can start after $\mu_c^i(t)$ is close to its asymptotic value looking at its convergence rate.

Theorem 2. *Consider the signal σ as defined in Definition 2 and a swarm of N robots with dynamics (1) whose sensing and communication topology is given by the undirected and connected graph \mathcal{G} . Assume that the initial deployment $x(0)$ is non-degenerate; then the closed-loop system (23) solves Problem 1 given the conditions of Proposition 1 for an annulus shell \mathcal{S} around p_σ and suitable constants ϵ_x and $\epsilon_\mu < 1$.*

Proof. We now justify the existence and appropriate selection of the time-scale parameters ϵ_x and ϵ_μ in the slow-fast closed-loop system (23) by following [33, Theorem 11.4]. To this end, we begin by unrolling the closed-loop system (23). Firstly, we note that the estimation of the centroid-relative coordinates x_i is exponentially stable, as established in Proposition 6. In particular, when the input signals $(x_i - x_j)$ vary slow enough, the estimation error of \hat{x}_i remains bounded [32]. This condition is satisfied when ϵ_x is chosen to be sufficiently small, ensuring that the estimator operates on a faster timescale than the state dynamics. Secondly, the estimation of the ascending direction

$\frac{\mu_c}{\|\mu_c\|}$ is also exponentially stable, according to Proposition 7. Again, for the estimation error in $\hat{\mu}_i$ to remain bounded, ϵ_μ must be chosen sufficiently small so that the estimator adapts faster than the variation in the inputs $(\mu_i - \mu_j)$, which in turn depend on the sensor readings $\sigma(p_i)$. The rate of change in $\sigma(p_i)$ is influenced by both the motion of the agents and the smoothness of the scalar field. If the estimation of \hat{x}_i is fast and its error remains bounded, then the estimation error in $\hat{\mu}_i(t)$ will also be bounded, as will the error in $\mu_c^i(t)$. It is important to note that $\mu_c^i(t)$ does not necessarily need to be estimated faster than $\hat{x}_i(t)$, depending on the relative rates of variation of $\sigma(p_i)$ and p_i . Since these variables are coupled, a rapid change in p_i may induce rapid variation in $\sigma(p_i)$, depending on the smoothness of the scalar field. Finally, note that although all the $\mu_c^i(t)$ converge to the same value $\mu(t)$, they are not exactly equal; nevertheless, the formation controller maintains the cohesion of the robot swarm. Also observe that the formation controller u_f exhibits exponential convergence properties as well, allowing us to treat it as a *vanishing disturbance* for the velocity that the robots are meant to track, i.e., the ascending direction.

In conclusion, in we define $\delta(t)$ as the angle deviation from the actual tracked direction by the centroid of the swarm and the ascending direction $\frac{\mu_c(t)}{\|\mu_c(t)\|}$, all the accumulated estimation errors result in a $\delta(t) \neq 0$ in general, but $\delta(t) \leq \epsilon_\delta \in \mathbb{R}^+$ remains bounded. The more conservative the constants ϵ_x and ϵ_μ are chosen, the smaller the bound ϵ_δ becomes, ensuring that $\dot{p}_c(t) \rightarrow R(\delta(t)) \frac{\mu_c(t)}{\|\mu_c(t)\|}$ remains an ascending direction within an annulus shell centered at p_σ where the gradient does not vanish and the variation of the scalar field is bounded. Therefore, following the same reasoning from Theorem 1, the closed-loop system (23) solves Problem 1 considering an annulus shell \mathcal{S} centered at p_σ . \square

V. SOURCE-SEEKING WITH CONSTANT-SPEED 2D UNICYCLE ROBOTS

We continue our analysis with a robot swarm consisting of 2D unicycle robots traveling at a constant common speed, modeled as in (2). For the sake of conciseness, in this section, we will show that the tracking of L_σ can be achieved exponentially fast by the unicycles so that it can be integrated seamlessly in the architecture of Figure 6, of course, accounting for the accumulated errors as we have done for system (23).

While we will consider the direction of L_σ , technically serving as the guiding vector for the robot swarm, it differs in two significant ways from other guiding vector fields [9], [10], [34]. Firstly, the field constructed from $L_\sigma(p_c, x)$ not only depends on the point p_c but also on the deployment x , which generally varies during the initial time and can be deliberately morphed for maneuvering purposes. Moreover, during this initial transitory, the centroid p_c may deviate until all the unicycles are well aligned with the desired direction. Secondly, since the signal σ is unknown, the robot swarm cannot determine the rate of change of L_σ throughout the field. As a result, it cannot be compensated for by a feed-forward term in the control action ω_i in (2) [9], [10], [34].

To address these challenges, we will consider first the always-ascending L_σ^1 for the analysis and subsequently analyze the

worst case scenario by considering L_σ as a bounded deviation from the ideal direction L_σ^1 . Let us define the set $U := \{p \in \mathbb{R}^{2N} \mid L_\sigma^1(p) \neq 0\}$ and introduce $m_d : U \rightarrow \mathbb{S}^1$ as

$$m_d(p) = \frac{L_\sigma^1(p)}{\|L_\sigma^1(p)\|} = [\cos(\alpha_d(p)) \quad \sin(\alpha_d(p))]^\top, \quad (24)$$

where $\alpha_d \in \mathbb{T}$ and $m_d(p)$ is the *vector field* that must be tracked at p_c to approach the source of the scalar field σ .

A. Aligning a team of 2D unicycle robots to the vector field of ascending directions

The objective of this section is to design $\omega_i, \forall i \in \mathcal{V}$ in (2) such that $m_i(\alpha_i) = [\cos \alpha_i \quad \sin \alpha_i]^\top \in \mathbb{S}^1$ aligns with m_d sufficiently close. To quantify this alignment, we define the signed angle between m_d and m_i as

$$\delta_i(p, \alpha_i) := \text{atan2}((Em_i)^\top m_d, m_i^\top m_d) \in \mathbb{T},$$

with E being a $+\frac{\pi}{2}$ rotation matrix. The function δ_i is defined wherever m_d is defined and is continuously differentiable (C^1) whenever $m_i(\alpha_i) \neq -m_d(p)$. Note that the time derivative of δ_i leads to

$$\dot{\delta}_i = \dot{\alpha}_i - \dot{\alpha}_d = \omega_i - \omega_d, \quad (25)$$

where $\omega_d := \|\dot{m}_d\|$, i.e., $\dot{m}_d = -\omega_d E m_d$.

Our goal is to achieve $\lim_{t \rightarrow \infty} \delta_i(t) = 0$, or at least to bound the tracking error effectively. To this end, we adopt the strategy proposed in [34], which involves using a proportional controller but this time without a feed-forward term, i.e.,

$$\omega_i(t) = -k_\gamma \delta_i(t), \quad (26)$$

where $k_\gamma \in \mathbb{R}^+$ is a control gain.

Lemma 5. *Let each robot $i \in \mathcal{V}$ be modeled as in (2) with ω_i in (26). Then, the following bound holds*

$$\|x_i(t) - x_i(0)\| \leq \frac{N-1}{N} \left(\frac{2\pi}{\kappa_\gamma} \right), \forall i \in \mathcal{V}. \quad (27)$$

Proof. See Subsection A in the Appendix. \square

Considering the control law (26), Lemma 5 provides a way to measure the *deformation* of the deployment concerning its initial condition. In particular, a larger gain κ_γ results in smaller eventual deformation. Hence, if $x(0)$ is non-degenerated, then $x(t) \rightarrow x^*$, where $x^* \in \mathbb{R}^{2N}$ is non-degenerated for a sufficiently large κ_γ . The required magnitude of κ_γ can be estimated using the minimum eigenvalue of the deployment's covariance matrix $P(x)$. Note that we have normalized the speed of the unicycle to 1 in (2); therefore, depending on the robot speed or length units, the deformation is directly proportional to such quantity.

Substituting (26) into (25) yields

$$\dot{\delta}_i(t) = \omega_i(t) - \omega_d(t) = -k_\gamma \delta_i(t) - \omega_d(t), \quad (28)$$

however, the robot swarm does not have knowledge of ω_d , as the signal σ is unknown in the source-seeking problem. We will design κ_γ by treating the upper bound of $|\omega_d(p)|$ as a non-vanishing bounded perturbation. However, $|\omega_d(p)|$ is not globally bounded, as the vector field $m_d(p)$ is not

well-defined for $p \in \{p : p_c = p_\sigma\}$ because $\nabla\sigma(p_\sigma) = 0$. Furthermore, in a neighborhood of such a set, ω_d changes rapidly; e.g., when p_c crosses p_σ the vector field $m_d(p)$ spins π radians *instantaneously*. Nevertheless, focusing our analysis on trajectories that remain outside this critical neighborhood still ensures that the robot swarm approaches the source, as required by Problem 1. In the following technical result, we prove for such trajectories that an upper bound for $|\omega_d(p)|$ always exists.

Lemma 6. *Let each robot $i \in \mathcal{V}$ be modeled as in (2) with ω_i in (26) and $x(0)$ non-degenerated. Then, for a given $\epsilon > 0$, there exist a constant $\kappa > 0$ and a function $\Omega_d(\epsilon) : \mathbb{R}^+ \rightarrow \mathbb{R}$ such that, if $\kappa_\gamma \geq \kappa$ and $\|\nabla\sigma(p_c(t))\| \geq \epsilon$, it holds that $|\omega_d(p(t))| < \Omega_d(\epsilon)$.*

Proof. See Subsection B in the Appendix. \square

Similar to the result in [33, Lemma 9.2] on bounded disturbances, having $|\omega_d(p)|$ uniformly bounded by Lemma 6, the following technical result shows how to design k_γ to ensure that all δ_i remain within a bounded interval after some finite time; i.e., the team of 2D unicycles aligns with the vector field $m_d(p)$ sufficiently close.

Proposition 8. *Let each robot $i \in \mathcal{V}$ be modeled as in (2) with ω_i in (26) and $x(0)$ non-degenerated. Then, for any given angle $\gamma \in (0, \frac{\pi}{2})$ and $\epsilon > 0$, there exist a constant $\kappa > 0$ and a finite time $T \in \mathbb{R}^+$ such that if $\kappa_\gamma > \kappa$ and $\|\nabla\sigma(p_c(t))\| > \epsilon, \forall t \in [0, T)$ then $|\delta_i(T)| < \gamma, \forall i \in \mathcal{V}$. Furthermore, this bound remains valid $\forall t \in [T, T^*)$, where $T^* \geq T$ denotes the first time such that $\|\nabla\sigma(p_c(T^*))\| \leq \epsilon$.*

Proof. See Subsection C in the Appendix. \square

B. Solution to the source-seeking problem for a team of 2D unicycle robots with a constant common speed

All the technical results in the previous subsections are not so relevant in practice, but they are just for formal analysis. Indeed, having $x(t)$ degenerated in real applications is practically impossible due to disturbances or error measurements. Considering a signal as defined in Definition 2, the variation of $\nabla\sigma(p_c)$ due to the robots' movement is sufficiently small and, in any case, can be bounded as shown in Lemma 6, at least far enough from the source. However, once the centroid of the swarm is close to the source, it can change rapidly, and they might not track the guiding vector field. Nonetheless, the robot swarm will repeatedly fall into a neighborhood close to the source while the deployment $x(t)$ converges exponentially fast to a fixed one close to $x(0)$. Note that, unlike the single-integrator controller, the shape of the deployment is not explicitly under control. As a result, although the final formation remains non-degenerate, its exact shape is arbitrary.

Theorem 3. *Let σ being a signal according to Definition 2. Consider a robot swarm of N constant-speed 2D unicycle robots modeled by (2), with a non-degenerated initial deployment $x(0)$, and $\|p_c(0) - p_\sigma\| > 0$. Then, given an $\epsilon > 0$ under the conditions of Lemma 6, there exists a $\kappa_\gamma > 0$ such that the control law $\omega_i = -\kappa_\gamma \delta_i, \forall i \in \mathcal{V}$, provides a solution to Problem 1.*

Proof. We will show that there exist a positive gain κ_γ for the angular velocity controller of the unicycles such that the centroid trajectory $p_c(t)$ stays within the set $\mathcal{B} := \{y \in \mathbb{R}^2 : \|y - p_\sigma\| < \epsilon_p\}$. Before proceeding, let us define $\mathcal{X} \subset \mathbb{R}^{2N}$ as a compact set centered at $x(0)$ of non-degenerated deployments. By selecting $\kappa_\gamma = \kappa_1$, with κ_1 as in Lemma 5, we ensure that $x(t) \in \mathcal{X}$ for all $t \geq 0$, i.e., the deployment remains non-degenerated. Therefore, from Lemma 1 we know

$$\frac{L_\sigma^1(p_c(t), x(t))^\top \nabla\sigma(p_c(t))}{\|L_\sigma^1(p_c(t), x(t))^\top\| \|\nabla\sigma(p_c(t))\|} = \cos(\theta(t)) > 0,$$

hence, there exists a constant $\gamma > 0$ such that $|\theta(t) + \gamma| < \frac{\pi}{2}$ for all t as long as $p_c(t) \neq p_\sigma$.

Next, let us choose $\epsilon^* > 0$ small enough such that $\mathcal{A} := \{y \in \mathcal{B} : \|\nabla\sigma(y)\| \leq \epsilon^*\} \subset \mathcal{B}$ and $d = \text{dist}(\mathcal{A}, \mathbb{R}^2 \setminus \mathcal{B}) > 0$. By applying Proposition 8 with the chosen ϵ^* and a fixed γ , there exists a gain $\kappa_2 > 0$ such that if $\kappa_\gamma > \kappa_2$, then there exists a time $T > 0$ such that $|\delta_i| < \gamma$, i.e., $[\cos \alpha_i(t) \quad \sin \alpha_i(t)] \nabla\sigma(p_c(t)) > 0, \forall i \in \mathcal{V}$ and $\forall t > T$ until $\|\nabla\sigma(p_c(t))\| \leq \epsilon^*$. Hence, since these conditions are met, we have that $\sigma(p_c(t))$ is increasing, as

$$\begin{aligned} \frac{d}{dt} \sigma(p_c(t)) &= \left(\frac{dp_c(t)}{dt} \right)^\top \nabla\sigma(p_c(t)) \\ &= \frac{1}{N} \sum_{i=1}^N [\cos \alpha_i(t) \quad \sin \alpha_i(t)] \nabla\sigma(p_c(t)) > 0. \end{aligned}$$

Therefore, similarly to Theorem 1, we have that the robot swarm will travel towards the source p_σ until it eventually enters the set \mathcal{A} . In case $p_c(t)$ exits \mathcal{A} , if we have $\kappa_\gamma \geq \kappa_3 = \max\{\kappa_1, \frac{2\Omega_d}{\gamma}, \frac{2}{d} \ln\left(\frac{\pi}{\gamma}\right)\}$, then $|\delta_i(t)| < \gamma, \forall i \in \mathcal{V}$ as in Proposition 8 before the robot swarm escapes \mathcal{B} , implying that the centroid reenters \mathcal{A} . Hence, by setting $\kappa_\gamma = \max\{\kappa_1, \kappa_2, \kappa_3\}$, we guarantee the trajectory of $p_c(t)$ remains within the set \mathcal{B} . In particular, there exists a time \bar{T} such that for all time $t > \bar{T}$, $\|p_c(t) - p_\sigma\| < \epsilon$ as required by Problem 1. \square

Remark 6. Note that by definition, the swarm of unicycle robots moves continuously, i.e., they move along orbits eventually of equal radii determined by the gain k_γ . \blacktriangleleft

Indeed, tracking the actual L_σ and not L_σ^1 by the robot swarm makes a deviation characterized by Lemma 2. However, as in Theorem 1, the solution to Problem 1 by Theorem 3 is still valid for a given $\|p_c(t) - p_\sigma\| < \epsilon$ with an extra bound for D considering the bound of the Hessian M and ϵ in Proposition 1. Of course, such a bound on D will be more relaxed for deployments considering L_σ^1 parallel to the gradient, i.e., for bigger deviations of L_σ due to a big D , we could still have $L_\sigma(p_c, x)^\top \nabla\sigma(p_c) > 0$ for longer time or convergence sets much closer to the source p_σ .

Remark 7. If the estimation of the ascending direction is obtained via the two consensus algorithms described in Figure 6, then the bounds given in Theorem 3 will be even more conservative since the centroid and ascending directions calculated distributively by the robots are not exactly the eventual asymptotic values considered in the main results. \blacktriangleleft

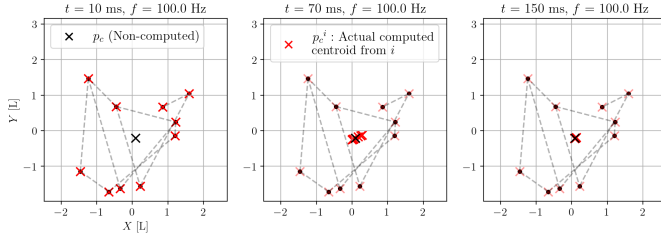


Fig. 7. Three snapshots from the algorithm in Proposition 6 that estimates the centroid of a robot swarm distributively. We can note the asymptotic convergence to the actual value of the centroid (X in black color), the X 's in red color are the values of $p_c^i(t) = p_i - \hat{x}_i(t)$. Each robot starts with $\hat{x}_i(0) = 0$ which is equivalent to start from their own positions (X 's in light red color). Dashed lines indicate neighboring robot pairs.

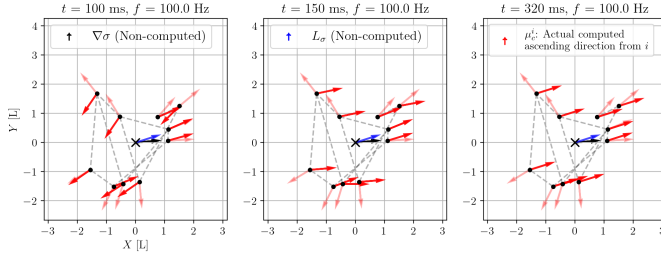


Fig. 8. Three snapshots from the algorithm in Proposition 7 that estimates the ascending direction at the centroid $L_\sigma / \|L_\sigma\|$ (blue arrow). The initials $\mu_c^i(0) = \mu_i(0) - \hat{\mu}_i(0)$, with $\hat{\mu}_i(0) = 0$, are in light red color, and eventually we can see how $\mu_c^i / \|\mu_c^i\|$ aligns with the ascending direction L_σ . Since only directional information is relevant, all vectors shown in this figure are normalized to a common magnitude. Dashed lines indicate neighboring robot pairs.

VI. NUMERICAL SIMULATIONS

All the numerical validations and simulations can be found in the following repository https://github.com/Swarm-Systems-Lab/source_seeking.

A. Distributed estimation of the swarm centroid and ascending direction

We provide numerical validation of Proposition 6 in Figure 7, and of Proposition 7 in Figure 8. The simulations are based on the following set of edges $\mathcal{E} = \{(0, 3), (0, 9), (3, 6), (0, 8), (8, 5), (6, 7), (1, 4), (4, 2), (8, 1), (9, 2), (5, 9)\}$, which corresponds to a graph with algebraic connectivity $\lambda_2 = 0.26$. In Figure 7, each robot asymptotically estimates the centroid of the swarm p_c relative to its own reference frame centered at p_i , i.e., the centroid-relative coordinates $-x_i$. In Figure 8, a similar estimation process is shown, but for the centroid of the directions μ_i , denoted by μ_c , which is parallel to the collective ascending direction L_σ .

B. Distributed source-seeking with single integrators

In Figure 9, we deploy 20 single-integrator robots modeled as in (23) and measuring the non-convex signal

$$\sigma(p) = k \frac{x_\sigma(p)}{\|x_\sigma(p)\|} - Q_a(x_\sigma(p) - a) \exp\{(x_\sigma(p) - a)^\top Q_a(x_\sigma(p) - a)\} - Q_b(x_\sigma(p) - b) \exp\{(x_\sigma(p) - b)^\top Q_b(x_\sigma(p) - b)\}, \quad (29)$$

where $x_\sigma(p) := (p - p_\sigma)/\delta$, $\delta = 15$, $k = 0.04$, $a = \begin{bmatrix} 1 \\ 0 \end{bmatrix}$, $b = \begin{bmatrix} 0 \\ -1.5 \end{bmatrix}$, $p_\sigma = \begin{bmatrix} 40 \\ 40 \end{bmatrix}$, $Q_a = 0.9 \begin{bmatrix} \frac{1}{\sqrt{30}} & 0 \\ 0 & 1 \end{bmatrix}$, $Q_b = -A^\top S A$, with $A = \frac{1}{\sqrt{2}} \begin{bmatrix} 1 & -1 \\ 1 & 1 \end{bmatrix}$ and $S = 0.9 \begin{bmatrix} 1 & 0 \\ 0 & \frac{1}{\sqrt{15}} \end{bmatrix}$. Both, the centroid and the ascending direction are calculated distributively, using $\epsilon_x = 0.5$ and $\epsilon_\mu = 0.001$. The underlying formation controller consider x_d as the initial formation and try to preserve it with $k_f = 0.1$. This initial formation is a uniform rectangular distribution. Eventually, the centroid swarm gets so close to the source that L_σ becomes unreliable, i.e., the centroid entered the ϵ -ball in Problem 1.

In Figure 10, the same scalar field in (29) is considered, but this time $\delta = 20$, $k = 0.06$, $a = \begin{bmatrix} 1.5 \\ 0 \end{bmatrix}$, $b = \begin{bmatrix} -1 \\ -1 \end{bmatrix}$, and $p_\sigma = \begin{bmatrix} 35 \\ -35 \end{bmatrix}$. This time we deploy 30 single-integrator robots, also modeled as in (23), but to validate the resilience of our source-seeking algorithm, we deliberately disconnect a robot every 3.75 T, so that at the end of the mission eight robots have been disconnected from the network while ensuring that the alive robots keep connected. Even though with the presence of dead robots, the alive agents eventually find the source of the scalar field.

C. Source-seeking with unicycles and a dynamic source

In Figure 11, we illustrate the effectiveness of Theorem 3 using 2D unicycle robots traveling at constant speed to track a dynamic scalar field source. Although the agents begin with arbitrary headings, they converge to a common direction closely aligned with the one defined by L_σ . Notably, once the swarm centroid approaches the source, the robots begin to describe close orbits, thereby bounding the distance between the centroid and the source.

VII. CONCLUSION

We have presented a fully distributed methodology to solve the source seeking problem with robot swarms by dynamically estimating both the centroid and an ascending direction using consensus-based algorithms, assuming single-integrator dynamics. Unlike previous methods, our approach does not require strict formation constraints, allowing for deformable swarm shapes and enabling shape morphing during motion. For unicycle dynamics, we have demonstrated a centralized solution that remains effective despite more restrictive kinematic constraints. Theoretical results were supported by extensive simulations, validating the convergence properties and robustness of our approach under a variety of conditions.

Future work will deepen the analysis of the distributed system, quantifying the impact of imperfect measurements, and the trade-offs between estimation speed, agent velocity, and scalar field smoothness to ensure more accurate convergence. These insights will guide the specification of practical requirements, helping us to implement the algorithm in the real world using custom hardware designed to meet the computational and communication demands identified by our analysis. Furthermore, we aim to extend our results to 3D unicycle robots, where geometric $SO(3)/SE(3)$ -based control laws will be developed to align spatially constrained agents, extending our framework to more complex environments.

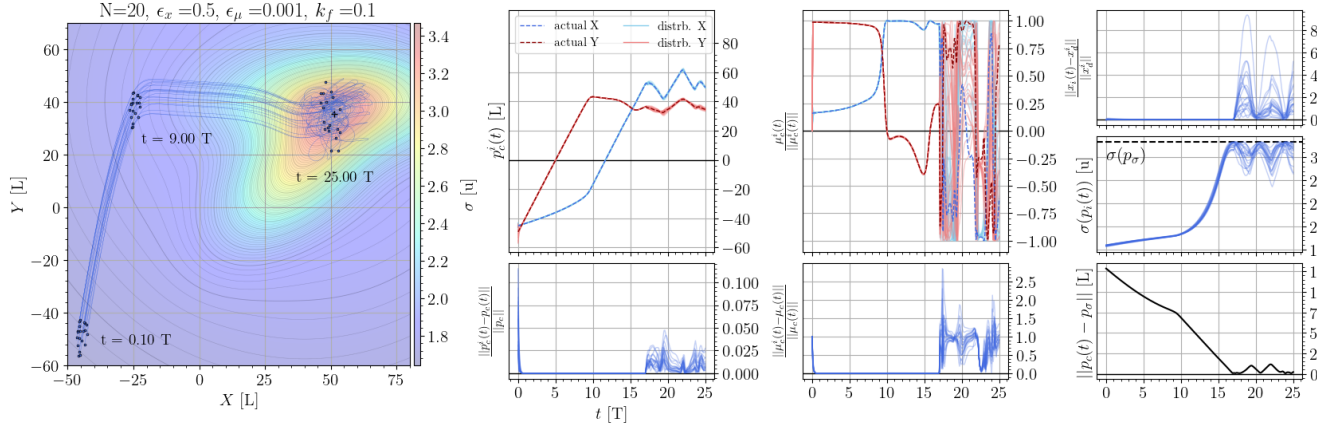


Fig. 9. A swarm of 30 single-integrator robots (blue dots), modeled by the slow-fast closed-loop system (23). In the two middle columns: the right plot shows the estimated centroid $p_c^i(t) = p_i(t) - \hat{x}_i(t)$, with the corresponding mean deviation error displayed below; the left plot shows the evolution of the normalized estimated direction $\mu_c^i(t)/\|\mu_c^i(t)\|$, also accompanied by its mean deviation error. In the rightmost column, from top to bottom: the mean deviation error between the actual formation $x(t)$ and the desired one x_d ; the scalar signal readings of the robots (blue lines), with the source value indicated by a black dashed line; and the norm of the relative position between the robots and the source.

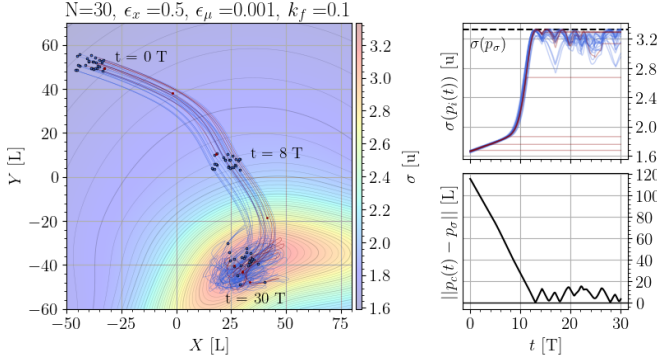


Fig. 10. A swarm of 30 single-integrator robots, modeled by the slow-fast closed-loop system (23). During the mission, 8 robots are deliberately disconnected at different time steps (red dots) to demonstrate that the remaining *alive* robots (blue dots) successfully reach the source, highlighting the swarm's resiliency. On the right, from top to bottom, the signal readings of the robots are shown, with the source value indicated by a black dashed line. Below, the norm of the relative position between the robots and the source; disconnected robots are excluded from the computation of $p_c(t)$.

APPENDIX

A. Proof of Lemma 5

Proof. Let us define $\delta_{ij} := \alpha_i - \alpha_j$, which is the oriented angle from the heading of robot i towards the heading of robot j , so that $\delta_{ij} \in (-2\pi, 2\pi)$ and if $\delta_{ij} = 0$, then robots i and j share the same heading. Note that $\delta_{ij} = \delta_i - \delta_j$; hence

$$\dot{\delta}_{ij} = \omega_i - \omega_j = -\kappa_\gamma(\delta_i - \delta_j) = -\kappa_\gamma\delta_{ij},$$

whose trajectory can be described by $\delta_{ij}(t) = \delta_{ij}(0)e^{-\kappa_\gamma t}$, thus we have that $\lim_{t \rightarrow \infty} \delta_{ij} = 0$. Now we are ready to (over)estimate the deformation of the relative positions concerning their initial states. We start by considering

$$\begin{aligned} \dot{p}_{ij} &= \dot{p}_i - \dot{p}_j = \begin{bmatrix} \cos \alpha_i & -\sin \alpha_i \\ \sin \alpha_i & \cos \alpha_i \end{bmatrix} \begin{bmatrix} v_i \\ \omega_i \end{bmatrix} - \begin{bmatrix} \cos \alpha_j & -\sin \alpha_j \\ \sin \alpha_j & \cos \alpha_j \end{bmatrix} \begin{bmatrix} v_j \\ \omega_j \end{bmatrix} \\ &= 2 \sin \left(\frac{\delta_{ij}}{2} \right) \begin{bmatrix} -\sin \left(\frac{\alpha_i + \alpha_j}{2} \right) \\ \cos \left(\frac{\alpha_i + \alpha_j}{2} \right) \end{bmatrix} = 2 \sin \left(\frac{\delta_{ij}(0)e^{-\kappa_\gamma t}}{2} \right) \begin{bmatrix} -\sin \left(\frac{\alpha_i + \alpha_j}{2} \right) \\ \cos \left(\frac{\alpha_i + \alpha_j}{2} \right) \end{bmatrix}, \end{aligned}$$

which leads to the inequality

$$\|\dot{p}_{ij}(t)\| \leq 2 \left| \sin \left(\frac{\delta_{ij}(0)e^{-\kappa_\gamma t}}{2} \right) \right| \leq |\delta_{ij}(0)|e^{-\kappa_\gamma t},$$

Therefore, the relative positions stabilize exponentially fast. In fact, since $p_{ij}(t) = p_{ij}(0) + \int_0^t \dot{p}_{ij}(s) ds$ we conclude that

$$\begin{aligned} \|p_{ij}(t) - p_{ij}(0)\| &= \left\| \int_0^t \dot{p}_{ij}(s) ds \right\| \leq \int_0^t \|\dot{p}_{ij}(s)\| ds \leq \\ &\leq |\delta_{ij}(0)| \int_0^t e^{-\kappa_\gamma s} ds \leq |\delta_{ij}(0)| \int_0^\infty e^{-\kappa_\gamma s} ds = \frac{|\delta_{ij}(0)|}{\kappa_\gamma} \leq \frac{2\pi}{\kappa_\gamma}, \end{aligned}$$

where we have used $\delta_{ij}(0) \in (-2\pi, 2\pi)$.

Next, we observe that

$$x_i = p_i - \frac{1}{N} \sum_{j \in \mathcal{V}} p_j = \frac{1}{N} \sum_{j \in \mathcal{V}} (p_i - p_j) = \frac{1}{N} \sum_{j \in \mathcal{V} \setminus \{i\}} (p_i - p_j),$$

thus

$$\|x_i(t) - x_i(0)\| = \frac{1}{N} \sum_{j \in \mathcal{V} \setminus \{i\}} \|p_{ij}(t) - p_{ij}(0)\| \leq \frac{N-1}{N} \left(\frac{2\pi}{\kappa_\gamma} \right). \quad \square$$

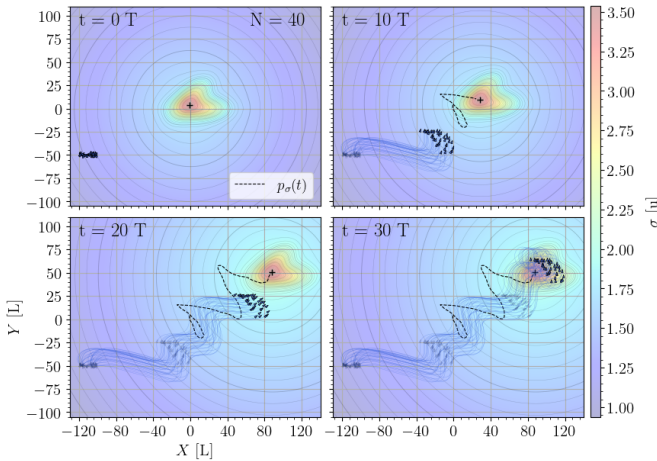


Fig. 11. A swarm of 40 2D unicycle robots (blue triangles) travelling at constant speed tracks a dynamic scalar field source, whose trajectory is shown by the dashed black line $p_\sigma(t)$. The swarm eventually reaches the source and begins to orbit around it.

B. Proof of Lemma 6

Before the main proof, first we need to provide the following technical result.

Lemma 7. *Let each robot $i \in \mathcal{V}$ be modeled as in (2) with ω_i in (26) and $x(0)$ non-degenerated. Then, there exist constant $\kappa > 0$ such that if $\kappa_\gamma \geq \kappa$, it holds that $\|L_\sigma^1(p_c(t), x(t))\| \geq \frac{\lambda_{\min}\{P(x(t))\}}{D^2} \|\nabla\sigma(p_c(t))\|$.*

Proof. Because $x(0)$ is non-degenerated, from Lemma 5 we know that there exist $\kappa > 0$ so that if $\kappa_\gamma > \kappa$ then $x(t), \forall t \geq 0$ is non-degenerated. Then, considering the lower bound of $L_\sigma^1(p_c, x)^\top \nabla\sigma(p_c)$ from Lemma 3 and the standard Cauchy–Schwarz inequality, we have that $\frac{\lambda_{\min}\{P(x)\}}{D^2} \|\nabla\sigma(p_c)\|^2 \leq L_\sigma^1(p_c, x)^\top \nabla\sigma(p_c) \leq \|L_\sigma^1(p_c, x)\| \|\nabla\sigma(p_c)\|$, which proves the claim. \square

Proof of Lemma 6. Since $\|m_d\|^2 = 1$, it follows from [35, Lemma 3.1] that $\omega_d(t) = \dot{m}_d(t)^\top E m_d(t)$. Consequently, $|\omega_d(t)| \leq \|\dot{m}_d(t)\| \|m_d(t)\| = \|\dot{m}_d(t)\|$. Therefore, bounding $|\omega_d(t)|$ reduces to bounding $\|\dot{m}_d(t)\|$.

From the definition of m_d in (24), we have

$$m_d = \frac{L_\sigma^1}{\|L_\sigma^1\|} = \frac{\sum_{i=1}^N (\nabla\sigma(p_c)^\top (p_i - p_c)(p_i - p_c))}{\|\sum_{i=1}^N (\nabla\sigma(p_c)^\top (p_i - p_c)(p_i - p_c))\|}.$$

Calculating the time derivative of one term in the sum gives

$$\begin{aligned} \frac{d}{dt} (\nabla\sigma(p_c)^\top (p_i - p_c)(p_i - p_c)) &= \\ &= [(H_\sigma(p_c) \dot{p}_c)^\top (p_i - p_c) + \nabla\sigma(p_c)^\top (\dot{p}_i - \dot{p}_c)] (p_i - p_c) \\ &\quad + \nabla\sigma(p_c)^\top (p_i - p_c)(\dot{p}_i - \dot{p}_c). \end{aligned} \quad (30)$$

Regarding the different terms in (30), from Lemma 5, we know that $\|p_i - p_c\| = \|x_i\| \leq \frac{2\pi}{\kappa_\gamma} + \|x_i(0)\| \leq M_1$. Additionally, we have that $\|\dot{p}_i - \dot{p}_c\| = \|\dot{p}_i - \frac{1}{N} \sum_{j=1}^N \dot{p}_j\| \leq 1$, and, indeed, we also have that $\|\dot{p}_c\| \leq 1$. Finally, we remind that the Hessian and the gradient of σ are also bounded by Definition 2. Hence, it follows that

$$\left\| \frac{dL_\sigma^1(p_c, x)}{dt} \right\| \leq NM_1(MM_1 + 2K) \leq C_1^*,$$

for some global constant $C_1^* > 0$. Furthermore, since $\frac{d}{dt} \|L_\sigma^1\| = \frac{1}{2\|L_\sigma^1\|} \frac{d}{dt} \|L_\sigma^1\|^2 = \dot{L}_\sigma^1{}^\top \frac{L_\sigma^1}{\|L_\sigma^1\|}$, we also have that

$$\frac{d}{dt} \|L_\sigma^1\| \leq \left\| \frac{dL_\sigma^1(p_c, x)}{dt} \right\| \leq C_1^*.$$

Combining all the (conservative) calculated bounds, we can conclude that $|w_d| \leq \left\| \frac{d}{dt} m_d \right\| \leq \frac{2C_1^* \|L_\sigma^1\|}{\|L_\sigma^1\|^2} = \frac{2C_1^*}{\|L_\sigma^1\|} \leq \frac{2C_1^*}{m\epsilon} = \Omega_d$, where for the last inequality we have chosen $\kappa_\gamma \geq \kappa$ from Lemma 7 so that $x(t)$ is non-degenerated, and together with the assumption $\|\nabla\sigma(p_c(t))\| \geq \epsilon$ we can choose m from Lemma 7 as well. \square

C. Proof of Proposition 8

Proof. Due to Lemma 6 we have that if $\nabla\sigma(p_c(t)) > \epsilon$, then $|\omega_d| \leq \Omega_d$ for all t , i.e., $|\omega_d| \leq \Omega_d, \forall t \in [0, T]$. Consequently, we consider $\kappa_\gamma \geq \kappa = \max \left\{ \kappa^*, \frac{2\Omega_d}{\gamma}, \frac{2}{T} \ln \left(\frac{\pi}{\gamma} \right) \right\}$, where κ^* is chosen according to Lemma 5 so that $x(t)$ is non-degenerated.

Given this choice of κ_γ , we firstly analyze the behavior of δ_i . If $\delta_i \geq \gamma$ then $\dot{\delta}_i \leq -\kappa_\gamma \delta_i + \Omega_d \leq -\kappa_\gamma \delta_i + \kappa_\gamma \frac{\delta_i}{2}$. Similarly, if $\delta_i \leq -\gamma$, we obtain $\dot{\delta}_i \geq -\kappa_\gamma \delta_i - \Omega_d \geq \kappa_\gamma \frac{\delta_i}{2}$. Thus, the interval $I := (-\gamma, \gamma)$ is attractive. In particular, given the uniqueness of solutions, once $\delta_i(t)$ enters I , it remains as long as the conditions of Lemma 6 are fulfilled; that is, until the first time $T^* \geq T$ such that $\|\nabla\sigma(p_c(T^*))\| \leq \epsilon$. \square

- [1] P. Ogren, E. Fiorelli, and N. E. Leonard, "Cooperative control of mobile sensor networks: Adaptive gradient climbing in a distributed environment," *IEEE Transactions on Automatic control*, vol. 49, no. 8, pp. 1292–1302, 2004.
- [2] V. Kumar, D. Rus, and S. Singh, "Robot and sensor networks for first responders," *IEEE Pervasive computing*, vol. 3, no. 4, pp. 24–33, 2004.
- [3] K. McGuire, C. De Wagter, K. Tuyls, H. Kappen, and G. C. de Croon, "Minimal navigation solution for a swarm of tiny flying robots to explore an unknown environment," *Science Robotics*, vol. 4, no. 35, p. eaaw9710, 2019.
- [4] W. Li, J. A. Farrell, S. Pang, and R. M. Arrieta, "Moth-inspired chemical plume tracing on an autonomous underwater vehicle," *IEEE Transactions on Robotics*, vol. 22, no. 2, pp. 292–307, 2006.
- [5] J. N. Twigg, J. R. Fink, L. Y. Paul, and B. M. Sadler, "Rss gradient-assisted frontier exploration and radio source localization," in *2012 IEEE International Conference on Robotics and Automation*. IEEE, 2012, pp. 889–895.
- [6] G.-Z. Yang, J. Bellingham, P. E. Dupont, P. Fischer, L. Floridi, R. Full, N. Jacobstein, V. Kumar, M. McNutt, R. Merrifield *et al.*, "The grand challenges of science robotics," *Science robotics*, vol. 3, no. 14, p. eaar7650, 2018.
- [7] M. Brambilla, E. Ferrante, M. Birattari, and M. Dorigo, "Swarm robotics: a review from the swarm engineering perspective," *Swarm Intelligence*, vol. 7, pp. 1–41, 2013.
- [8] M. Dorigo, G. Theraulaz, and V. Trianni, "Swarm robotics: Past, present, and future [point of view]," *Proceedings of the IEEE*, vol. 109, no. 7, pp. 1152–1165, 2021.
- [9] W. Yao, H. G. de Marina, B. Lin, and M. Cao, "Singularity-free guiding vector field for robot navigation," *IEEE Transactions on Robotics*, vol. 37, no. 4, pp. 1206–1221, 2021.
- [10] W. Yao, H. G. de Marina, Z. Sun, and M. Cao, "Guiding vector fields for the distributed motion coordination of mobile robots," *IEEE Transactions on Robotics*, 2022.
- [11] E. Rosero and H. Werner, "Cooperative source seeking via gradient estimation and formation control," in *2014 UKACC International Conference on Control (CONTROL)*. IEEE, 2014, pp. 634–639.
- [12] S. A. Barogh and H. Werner, "Cooperative source seeking with distance-based formation control and non-holonomic agents," *IFAC-PapersOnLine*, vol. 50, no. 1, pp. 7917–7922, 2017.
- [13] L. Briñón-Arranz, L. Schenato, and A. Seuret, "Distributed source seeking via a circular formation of agents under communication constraints," *IEEE Transactions on Control of Network Systems*, vol. 3, no. 2, pp. 104–115, 2015.
- [14] L. Briñón-Arranz, A. Renzaglia, and L. Schenato, "Multirobot symmetric formations for gradient and hessian estimation with application to source seeking," *IEEE Transactions on Robotics*, vol. 35, no. 3, pp. 782–789, 2019.
- [15] R. Fabbiano, F. Garin, and C. Canudas-de Wit, "Distributed source seeking without global position information," *IEEE Transactions on Control of Network Systems*, vol. 5, no. 1, pp. 228–238, 2016.
- [16] Z. Li, K. You, and S. Song, "Cooperative source seeking via networked multi-vehicle systems," *Automatica*, vol. 115, p. 108853, 2020.
- [17] J. Cochran and M. Krstic, "Nonholonomic source seeking with tuning of angular velocity," *IEEE Transactions on Automatic Control*, vol. 54, no. 4, pp. 717–731, 2009.
- [18] E. Biryk and M. Arcak, "Gradient climbing in formation via extremum seeking and passivity-based coordination rules," *Asian Journal of Control*, vol. 10, no. 2, pp. 201–211, 2008.
- [19] S. Al-Abri and F. Zhang, "A distributed active perception strategy for source seeking and level curve tracking," *IEEE Transactions on Automatic Control*, vol. 67, no. 5, pp. 2459–2465, 2021.
- [20] T. Zhang, V. Qin, Y. Tang, and N. Li, "Distributed information-based source seeking," *IEEE Transactions on Robotics*, 2023.

- [21] B. Bayat, N. Crasta, H. Li, and A. Ijspeert, "Optimal search strategies for pollutant source localization," in *2016 IEEE/RSJ International Conference on Intelligent Robots and Systems (IROS)*. IEEE, 2016, pp. 1801–1807.
- [22] M. S. Lee, D. Shy, W. R. Whittaker, and N. Michael, "Active range and bearing-based radiation source localization," in *2018 IEEE/RSJ International Conference on Intelligent Robots and Systems (IROS)*. IEEE, 2018, pp. 1389–1394.
- [23] J. Cortes, S. Martinez, T. Karatas, and F. Bullo, "Coverage control for mobile sensing networks," *IEEE Transactions on robotics and Automation*, vol. 20, no. 2, pp. 243–255, 2004.
- [24] J. Cortes, "Distributed kriged kalman filter for spatial estimation," *IEEE Transactions on Automatic Control*, vol. 54, no. 12, pp. 2816–2827, 2009.
- [25] A. Benevento, M. Santos, G. Notarstefano, K. Paynabar, M. Bloch, and M. Egerstedt, "Multi-robot coordination for estimation and coverage of unknown spatial fields," in *2020 IEEE international conference on robotics and automation (icra)*. IEEE, 2020, pp. 7740–7746.
- [26] A. Acuaviva, J. Bautista, W. Yao, J. Jimenez, and H. G. de Marina, "Resilient source seeking with robot swarms," in *2024 IEEE 63rd Conference on Decision and Control (CDC)*. IEEE, 2024, pp. 57–63.
- [27] F. Bullo, *Lectures on network systems*. Kindle Direct Publishing, 2020, vol. 1.
- [28] A. Clauset, C. R. Shalizi, and M. E. Newman, "Power-law distributions in empirical data," *SIAM review*, vol. 51, no. 4, pp. 661–703, 2009.
- [29] K.-K. Oh, M.-C. Park, and H.-S. Ahn, "A survey of multi-agent formation control," *Automatica*, vol. 53, pp. 424–440, 2015.
- [30] H. G. de Marina, "Maneuvering and robustness issues in undirected displacement-consensus-based formation control," *IEEE Transactions on Automatic Control*, vol. 66, no. 7, pp. 3370–3377, 2020.
- [31] H. Zhang, F. L. Lewis, and A. Das, "Optimal design for synchronization of cooperative systems: state feedback, observer and output feedback," *IEEE Transactions on Automatic Control*, vol. 56, no. 8, pp. 1948–1952, 2011.
- [32] S. S. Kia, B. Van Scoy, J. Cortes, R. A. Freeman, K. M. Lynch, and S. Martinez, "Tutorial on dynamic average consensus: The problem, its applications, and the algorithms," *IEEE Control Systems Magazine*, vol. 39, no. 3, pp. 40–72, 2019.
- [33] H. K. Khalil, *Nonlinear control*. Pearson New York, 2015.
- [34] Y. A. Kapitanyuk, A. V. Proskurnikov, and M. Cao, "A guiding vector-field algorithm for path-following control of nonholonomic mobile robots," *IEEE Transactions on Control Systems Technology*, vol. 26, no. 4, pp. 1372–1385, 2017.
- [35] Y. Kapitaniuk, "Motion control algorithms for mobile vehicles and marine crafts," Ph.D. dissertation, 2020.



Jose Hinojosa Hidalgo completed his B.S. degree in Computer Engineering from the University of Granada, Spain, in 2024. He is currently pursuing a M.S. in Data Science and Computer Engineering from the University of Granada.

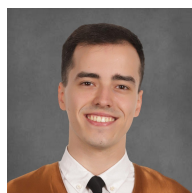


Weijia Yao received the Ph.D. degree in systems and control theory from the University of Groningen, Groningen, The Netherlands. His research interests include nonlinear systems and control, robotics, and multiagent systems. He was a Finalist for the Best Conference Paper Award from ICRA in 2021.



Juan Jimenez graduated in Physics from the Universidad Autónoma de Madrid (Spain) in 1986 and earned his Ph.D. in Systems Control in 1999 from the Universidad Nacional de Educación a Distancia (Spain). Since 2015, he has been an Associate Professor in the Department of Computer Architecture, Systems Engineering, and Automation at the Universidad Complutense de Madrid. His research interests include distributed control and cooperative control in multi-agent systems, with a particular focus on applications

to autonomous vehicles.



Jesus Bautista Villar (Student IEEE) received his B.S. degree in Physics from the Complutense University of Madrid, Spain, in 2022 and his M.S. degree in Data Science and Computer Engineering from the University of Granada, Spain, in 2023. He is currently pursuing a Ph.D. in Information and Communication Technologies, specializing in Cognitive Systems and Robotics, at the University of Granada, Spain.



Antonio Acuaviva earned his B.S. degrees in Mathematics and Physics from Universidad Complutense de Madrid, Spain, in 2022. He then obtained his M.A.St. in Mathematics from the University of Cambridge, UK, in 2023, supported by a 'la Caixa' Fellowship. Currently, he is pursuing his Ph.D. in Mathematics at Lancaster University, UK, where his research focuses on functional analysis and Banach space theory.



Hector Garcia de Marina (Member IEEE) received the Ph.D. degree in systems and control from the University of Groningen, The Netherlands, in 2016. He was a Postdoctoral Research Associate with the Ecole Nationale de l'aviation Civile, Toulouse, France, and an Assistant Professor with the Unmanned Aerial Systems Center, University of Southern Denmark, Odense, Denmark. Since 2022, he has been a Ramón y Cajal Researcher with the Department of Computer Engineering, Automation and Robotics, and with CITIC, Universidad de Granada, Spain. He is the recipient of an ERC Starting Grant and an Associate Editor for IEEE Transactions on Robotics. His current research interests include multiagent systems and the design of guidance navigation and control systems for autonomous vehicles.